

Master Dissertation

A Study of Dual-Band Power
Amplifier with Out-of-Band
Transmission Zeros

**대역외 전송 제로점을 갖는 이중 대역 전력
증폭기 설계**

2013. 02. 22

Graduate School of
Chonbuk National University

Division of Electronics and Information Engineering

Phirun Kim

A Study of Dual-Band Power Amplifier with Out-of-Band Transmission Zeros

**대역외 전송 제로점을 갖는 이중 대역 전력
증폭기 설계**

2013. 02. 22

Graduate School of
Chonbuk National University

Division of Electronics and Information Engineering

Phirun Kim

A Study of Dual-Band Power Amplifier with Out-of-Band Transmission Zeros

Academic Advisor: Professor Yongchae Jeong

A Dissertation Submitted In Partial Fulfillment of the
Requirements for the Degree
Master of Engineering

2012. 11. 07

Graduate School of
Chonbuk National University

Division of Electronics and Information Engineering

Phirun Kim

The Master dissertation of Phirun Kim

is approved by

Chair, Professor, Hae-Won Son
Chonbuk National University

Professor, Jung Mu Kim
Chonbuk National University

Advisor, Professor, Yongchae Jeong
Chonbuk National University

2012. 12. 13

Graduate School of
Chonbuk National University

To my beloved family

TABLE OF CONTENTS

DEDICATION	V
TABLE OF CONTENTS.....	Vi
LIST OF FIGURES	iX
LIST OF TABLES	Xiii
ABSTRACT	1
ABSTRACT IN KOREAN	2
ABBREVIATIONS	3
CHAPTER 1 INTRODUCTION.....	4
1.1 Literature Review	4
1.2 Dissertation Objectives and Organization	6
CHAPTER 2 POWER AMPLIFIER FUNDAMENTALS.....	7
2.1 RF Power Amplifier Basics	7
2.1.1 Design Class of Operation of Power Amplifier...	6
2.1.2 Class-A Operation	8
2.1.3 Reduced Conduction Angle Mode-	
Class- AB, B, C	8
2.1.4 Gain Match and Power Match.....	11
2.2 Dual-Band Bias Line	13
2.2.1 Dual-Band Bias Line Theory.....	14
2.2.2 Simulations and Measurements.....	16
2.3 Realized Inductor with a High Impedance	

Transmission Line	19
CHAPTER 3 DUAL-BAND IMPEDANCE	
MATCHING NETWORK	21
3.1 Design Theory	21
3.1.1 Derivation of Inductance and Capacitance in Dual-Band Matching	23
3.1.2 Conditions for Inductance and Capacitance	27
3.1.3 The Combination of T-type Matching Network and Auxiliary Combination of T-type Matching Network	30
CHAPTER 4 DESIGN DUAL-BAND AMPLIFIER WITH	
OUT-OF-BAND TRANSMISSION ZEROS	33
4.1 Optimizing the Impedance Matching	33
4.1.1 Impedance Matching at 0.881 GHz and 2.14 GHz	35
4.2 Realized Input Dual-Band M/N	39
4.2.1 T-type Single Band M/N	39
4.2.2 Lumped Elements Dual-Band Impedance M/N ..	41
4.2.3 Semi-Lumped Elements Dual-Band M/N	42
4.3 Realized Output Dual-Band M/N	44
4.3.1 T-type Single Band M/N	45
4.3.2 Lumped Elements Dual-Band Impedance M/N ..	47
4.3.3 Semi-Lumped Elements Dual-Band M/N	48

4.4 Dual-Band Amplifier	50
CHAPTER 5 CONCLUSION	57
REFERENCES	58

LIST OF FIGURES

Figure 2.1	Fourier analysis of reduced conduction angle current waveforms	9
Figure 2.2	Biasing points for class A, AB, B, and C.....	9
Figure 2.3	Block diagram of power amplifier	11
Figure 2.4	Compression characteristics for conjugate (S_{22}) match (solid curve) and power matching (dashed curve). The 1-dB compression point (B, B') and maximum linear power point (A, A') show improvements under power-matched conditions....	12
Figure 2.5	Conventional bias lines.....	13
Figure 2.6	Topology of dual-band bias line: (a) full structure and (b) equivalent circuit at f_2	15
Figure 2.7	Layout of dual-band bias line	16
Figure 2.8	The EM simulation of dual-band bias line	17
Figure 2.9	The photograph of proposed dual-band bias line ...	18
Figure 2.10	The measurement result of proposed dual-band bias line: (a) insertion loss and (b) output bias line	19
Figure 2.11	Transmission line and a lumped elements equivalent circuit.....	19
Figure 3.1	The combination of dual-band matching networks: (a) single band matching network at first band, (b) single band matching network at second band,	

	and (c) dual-band matching network.....	22
Figure 3.2	Characteristics of LC resonators and transmission zeros: (a) series-parallel resonator ($m=1$ or 3), (b) shunt-series resonator, and (c) transmission zero characteristic.....	24
Figure 3.3	The combinations of T-type matching network	31
Figure 3.4	The auxiliary combination of T-type matching network.....	32
Figure 4.1	The proposed structure of dual-band amplifier with out-of-band suppression	33
Figure 4.2	Load/source pull set up.....	34
Figure 4.3	The fabricated PCB of single band matching networks: (a) at 0.881 GHz and (b) at 2.14 GHz	36
Figure 4.4	Extracted impedances: (a) at 0.881 GHz and (b) at 2.14 GHz.....	37
Figure 4.5	Measured gain and efficiency according to output power at 0.881 GHz.....	38
Figure 4.6	Measured gain and efficiency according to output power at 2.14 GHz.....	38
Figure 4.7	Input T-type matching networks: (a) at 0.881 GHz and (b) at 2.14GHz.....	40
Figure 4.8	Simulation of source impedances: (a) at 0.881 GHz and (b) at 2.14 GHz	40

Figure 4.9	Input dual-band matching network	41
Figure 4.10	Simulation result of lumped elements input dual-band matching	42
Figure 4.11	The layout of proposed dual-band matching network	42
Figure 4.12	Photograph of fabricated PCB of input dual-band matching network	43
Figure 4.13	Extracted impedance and measurement impedance of input dual-band matching network.....	44
Figure 4.14	Output T-type matching networks: (a) at 0.881GHz and (b) at 2.14 GHz	45
Figure 4.15	Simulation results of load impedance: (a) at 0.881 GHz and (b) at 2.14 GHz	46
Figure 4.16	Output lumped elements dual-band matching network	47
Figure 4.17	Simulation result of output lumped elements dual-band matching	48
Figure 4.18	Layout of output dual-band matching network	48
Figure 4.19	The photograph of fabricated output dual-band matching network	49
Figure 4.20	The extracted impedance, simulation and measurement impedance of output dual-band matching network	50

Figure 4.21	Structure of dual-band amplifier with chip inductor DC bias	51
Figure 4.22	The proposed structure of dual-band amplifier with dual-band bias line.....	51
Figure 4.23	Photograph of the dual-band amplifier with bias inductor.....	52
Figure 4.24	Photograph of the dual-band amplifier with dual-band bias line.....	52
Figure 4.25	Measured gain and efficiency according to output power with operating frequency 0.881GHz	53
Figure 4.26	Measured gain and efficiency according to output power with operating frequency 2.14 GHz	54
Figure 4.27	Comparison of the measurement results between using chip inductor and dual-band bias line.....	55
Figure 4.28	Measurement of flatness characteristics: (a) at first band and (b) at the second band	56

LIST OF TABLES

Table 3.1	Condition of Series-Parallel LC	27
Table 3.2	Condition of Shunt-Series LC	28
Table 3.3	Analysis of LC Resonator	29
Table 4.1	Physical Layout of Input Dual-Band M/N.....	43
Table 4.2	Physical layout of Output Dual-Band M/N.....	49

ABSTRACT

Phirun Kim

Division of Electronics and Information Engineering

The Graduate School

Chonbuk National University

Modern wireless communication systems demand multi-band/multi-mode, efficient, and linear power amplifiers. This proliferation of wireless standard, operating over multiple frequencies bands, has increased the claim for radio frequency (RF) components, and consequently power amplifier (PA) to operate over multiple frequency bands. This multi-band PA can be operated several bands simultaneously with multi-band impedance matching network. In order to operate properly over the several bands, filters are used to suppress the unwanted signal at the out-of-bands.

This dissertation, dual-band power amplifier using a frequency limited dual-band impedance matching network is designed. The dual-band impedance matching network is realized with three LC resonators that can be able to match two different frequency bands and also able to present transmission zero to block the out-of band amplified noises and nonlinear components from the transistor.

Keywords: Single-band matching network, dual-band matching network, Power amplifier bias line.

ABSTRACT IN KOREAN

요약

현대의 무선 통신 시스템은 다중대역, 다중모드, 고효율 그리고 선형특성을 갖는 전력증폭기를 요구한다. 다중 주파수 대역에서 동작하는 무선통신기계의 확산이 RF 소자에 대한 요구가 증가시켰고, 그에 따라 다중 주파수 대역에서 동작하기 위한 전력증폭기의 요구 또한 증가했다. 이러한 다중대역 전력증폭기는 다중대역 임피던스 정합회로를 이용하여 동시에 여러 개의 대역에서 동작될 수 있다.

본 논문에서는 주파수 제한 이중대역 임피던스 정합회로를 이용한 이중대역 전력증폭기를 설계하였다. 이중대역 임피던스 정합회로는 두 개의 다른 주파수 대역을 정합할 수 있고 또한 트랜지스터에서 발생하는 잡음과 비선형 성분이 증폭되는 바깥쪽 대역을 차단하기 위한 전송 영점을 생기도록 하는 3 개의 LC 공진기를 이용하여 구현하였다.

주요어: 단일대역 정합회로, 이중대역 정합회로, 전력증폭기 바이어스 선로

ABBREVIATIONS

ADS	advanced design system
CRLH	composite right/left handed
DE	drain efficiency
DC	direct current
GSM	global system for mobile communications
HB	high band
IB	intermediate band
LB	low band
LC	inductor and capacitor
LHTL	left handed transmission line
MN	matching network
NRI	negative refractive index
PA	power amplifier
PAE	power added efficiency
PCB	print circuit board
RF	radio frequency
RHTL	right handed transmission line
TL	transmission line
TV	television
UHF	ultrahigh frequency
WCDMA	wideband code division multiple access

CHAPTER 1 INTRODUCTION

1.1 Literature Review

As a wireless communication system technology is advanced, an increasing number of communication standards have been proposed and implemented to meet the demand for a different application. Therefore, the requirements and the design target for a radio-frequency (RF) power amplifier (PA) include high efficiency, linearity, stability, multi-band, and broadband operational ability are very important for many wireless communication systems. The traditional PA design focuses mainly on one single frequency band. However, since multiple communication standards such as global system for mobile communications (GSM), wideband code division multiple access (WCDMA), long term evolution (LTE), etc., have been implemented to meet the demands for different applications in wireless communication systems. For a broadband PA, a wideband matching network (MN) topology is needed to achieve optimal impedance matching network within a wide frequency range. For multifunctional multi-band communication systems, PA have become a very challenging area because the PA should handle voice, data, and broadcast with global roaming capability. For the multi-band PA, a single band impedance matching network can not be sufficient to operate for all of bands. Therefore, the PAs should have a multi-mode/multi-band capability with high efficiency.

Structures such as multi-sections LC circuits [1] and tapered transmission lines [2] have shown their ability to achieve wideband matching network (M/N). For a multi-band PA, circuit topologies such as an impedance buffer [3][4], a multi-section impedance transformer [5], and T- and Pi-type stub loaded quarter-wave transformers [6] have been proposed to realize impedance matching network at multiple frequency bands. Among other solutions, the PA with a reconfigurable M/N designed for each specific frequency can be applied in both broadband and multi-band PA design. Also, it is found that choosing a proper class of operation with wider design space and less sensitivity of harmonic mismatch can help to less the restriction of broadband or multi-band matching and thus provide more flexibility in PA design [7]. A left handed transmission line (LHTL) or negative refractive index (NRI) transmission lines have been performed widely. Those metamaterial sections are implemented on planar circuits with normal right handed transmission lines (RHTL), because RHLT section play a very importance role of physical base in order for LHTL components to be attached or connected in circuits. So the LHTL structures are realized with the form of composite right/left handed (CRLH) transmission line structures. The design of dual-band power amplifier using composite right/left handed (CRLH) transmission line structure is mentioned in [8]-[10]. Usually, the CRLH transmission line section for the dual-band matching network is implemented by lumped inductors and capacitors as the left handed (LH) section, and normal transmission line elements as the right handed (RH) section. Within this topology the network is huge and expensive. In this dissertation, the dual-band matching network is realized with three LC resonators

that can match at both band simultaneously with out-of-band transmission zeros and small size.

1.3 Dissertation Objectives and Organization

The main objective of this dissertation is to design a dual-band power amplifier for the multifunctional wireless systems. Firstly, the dual-band matching network with three LC resonators is investigated in this work. This dual-band matching network can match two bands simultaneously and also provides transmission zeros with out-of-band. To realize LC resonators effectively, the lumped inductor elements of proposed dual-band matching network are implemented with distributed transmission lines.

The rest of this dissertation is organized as follows. Chapter 2 briefly describes the fundamental principle of RF power amplifier techniques and class operation. The gain matching and power matching are also mentioned. Moreover, the dual-band bias line for the dual-band power amplifier are analyzed, simulated, and measured. The Chapter 3 describes the design theory of dual-band impedance matching network. And Chapter 4 will present the whole process to designing of dual-band PA with dynamic range amplifier. Discussion covers with the optimizing the impedance of both bands and then realized dual-band matching with semi-lumped elements. The last of this chapter will present the performance of dual-band matching network with the out-of-band transmission zeros.

Finally, Chapter 5 summarizes the contributions of the dissertation.

CHAPTER 2 POWER AMPLIFIER FUNDAMENTALS

In this chapter, the basic RF operation due to bias conditions and gain match will be presented. Also, the derivation of dual-band bias line is mentioned with simulation and measurement.

2.1 RF Power Amplifier Basics

RF power amplifiers are used in various applications including wireless communication, TV transmission, radar, and RF heating. In order to ponder on the different types of amplifiers, figures of merit have to be defined. This will give an intuition of the benefits or disadvantages of applying a specific bias condition of amplifier. Conventionally, it is stated that a low-efficiency linear amplifier (class-A, class-AB) are convenient for non-constant-envelope signals while a high efficiency nonlinear amplifiers (class-E, class-F) are for constant-envelope signals. Nevertheless, current and advent mobile applications demand high efficiency and linear characteristic simultaneously. In practice, of course, the linear region will contain weak nonlinearities.

2.1.1 Bias Operation of Power Amplifier

Different bias operations of power amplifier can be employed for different design requirements and applications. General performance issues for PA design include gain, operation bandwidth, output power delivered to the load, drain

efficiency/power added efficiency, and linearizability, etc. The several classical bias operation of power amplifier will be introduced briefly in the following subsections.

2.1.2 Class A Operation

Class A is the only operation mode that allows a transistor to conduct for the full signal period. The output current waveform of class A is sinusoidal, which exactly follows the variation of the input voltage. Class A has a strong linear performance since the transistor is biased in the active linear region. The maximum drain efficiency of the ideal class A is only 50%. The low efficiency feature made class A operation as not a popular bias operation for the high efficiency PA design.

2.1.3 Reduced Conduction Angle Mode- Class- AB, B, C

Several bias operation modes have been proposed to improve the efficiency of amplifiers. The conventional high efficiency amplifier modes include Class AB, Class B, and Class C. The conduction angle is defined as the proportion of the RF cycle during which the transistor is conducting. Fig. 2.1 shows the current waveform of different conduction angles (α) for class A, B, AB, and C. A few harmonic amplitudes are also plotted in Fig. 2.1. Note that throughout the class AB range, and up to the midway class B condition, the largest harmonic, other than the fundamental, is the second. The conduction angle of drain current is reduced by lowering the gate biasing point so that the input voltage cycle drops below the threshold voltage and prevent the transistor from conducting current. Fig. 2.2 shows the biasing points of class A, B, AB, and C (assuming knee voltage is zero).

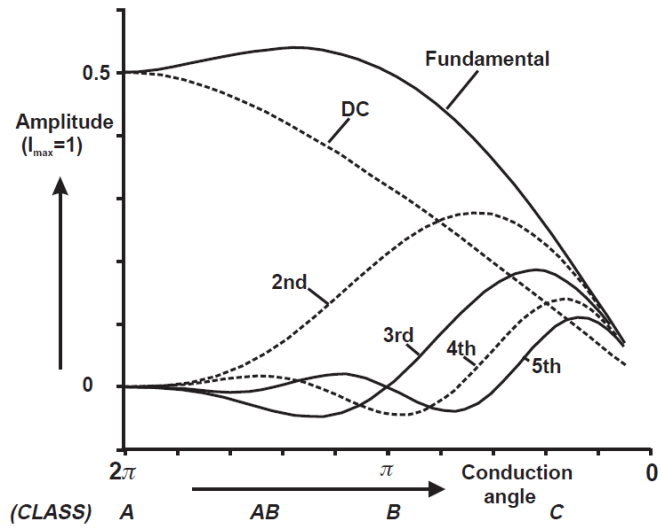


Fig. 2.1. Fourier analysis of reduced conduction angle current waveforms.

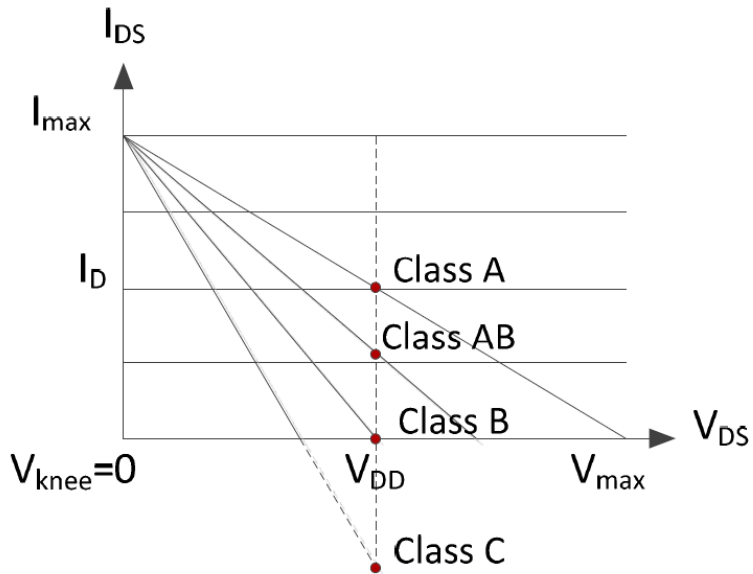


Fig. 2.2. Biasing points for class A, AB, B, and C.

Assuming the maximum current swing up to I_{max} and the maximum voltage swing up to V_{max} ($2V_{DD}$), the RF output power is

$$P_{out} = \frac{V_{DD}}{\sqrt{2}} \times \frac{I_1}{\sqrt{2}} . \quad (2.1)$$

The DC power consumption is given by

$$P_{DC} = V_{DD} \times I_{DC} . \quad (2.2)$$

Where I_1 and I_{DC} are the fundamental and DC components of drain current, respectively [11]. Using Fourier analysis the fundamental current can be obtained

$$I_1 = \frac{I_{max}}{2\pi} \times \frac{\alpha - \sin \alpha}{1 - \cos\left(\frac{\alpha}{2}\right)} \quad (2.3)$$

and

$$I_{DC} = \frac{I_{max}}{2\pi} \times \frac{2 \sin\left(\frac{\alpha}{2}\right) - \alpha \cos\left(\frac{\alpha}{2}\right)}{1 - \cos\left(\frac{\alpha}{2}\right)} . \quad (2.4)$$

The output efficiency (drain efficiency) is defined by

$$DE = \frac{P_1}{P_{DC}} . \quad (2.5)$$

Because the conduction angle of class AB operation mode is between class A ($\alpha=2\pi$) and class B ($\alpha=\pi$), the maximum efficiency of class AB is between 50% and 78.5%. The class AB operation provides the opportunity to balance the tradeoff between linearity and efficiency.

Class C amplifier is biased more deeply than class B amplifier and thus has a smaller conduction angle of current waveform. The drain efficiency of class C can be higher than 78.5%; however, class C amplifier suffers more from nonlinearity issues. In order to get I_{max} , more input voltage is needed if the operation mode has

lower gate biasing, and it can be seen that the achievable gain reduces as we shift from class A to class C.

2.1.4 Gain Match and Power Match

Fig. 2.3 shows the block diagram of amplifier. The ratio of output RF power to input the dissipated DC power called drain efficiency (DE) as describe in (2.5).

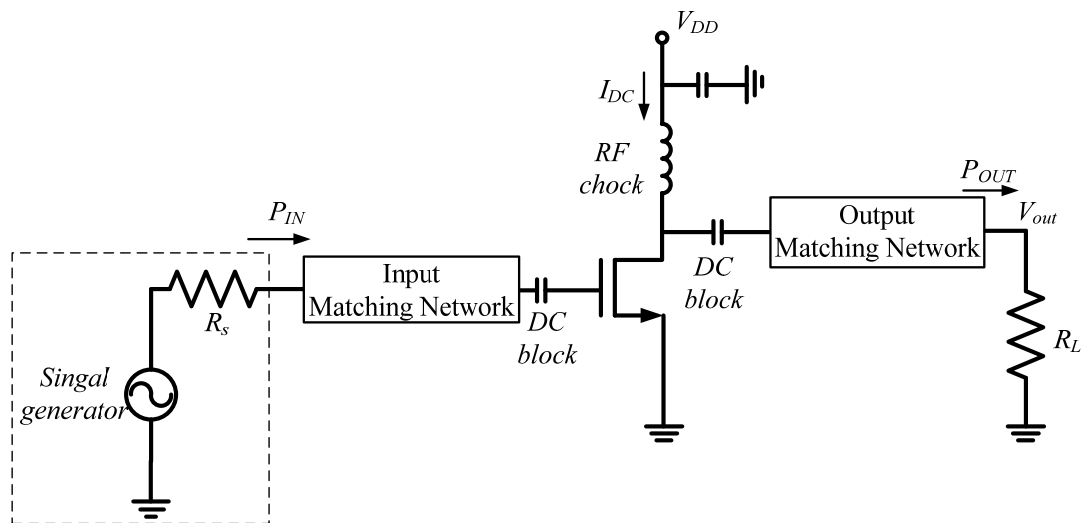


Fig. 2.3. Amplifier block diagram.

Since the amplifier amplifies the fed input signal, a more inclusive definition for power efficiency should also include the effect of input power. A power added efficiency (PAE) was introduced as equation (2-6). The PAE is always less than DE.

$$PAE = \frac{P_{LOAD} - P_{IN}}{P_{DC}} \quad (2.6)$$

Transistor gain is highly dependent on the drain current, and at high power it drops quickly. Fig. 2.4 shows the power transfer characteristic of a class A amplifier with two different output matching conditions. The solid line shows the response for the amplifier which has been conjugately matched at much lower drive levels. The two points A and B refer to the maximum linear power and the 1 dB compression power, respectively.

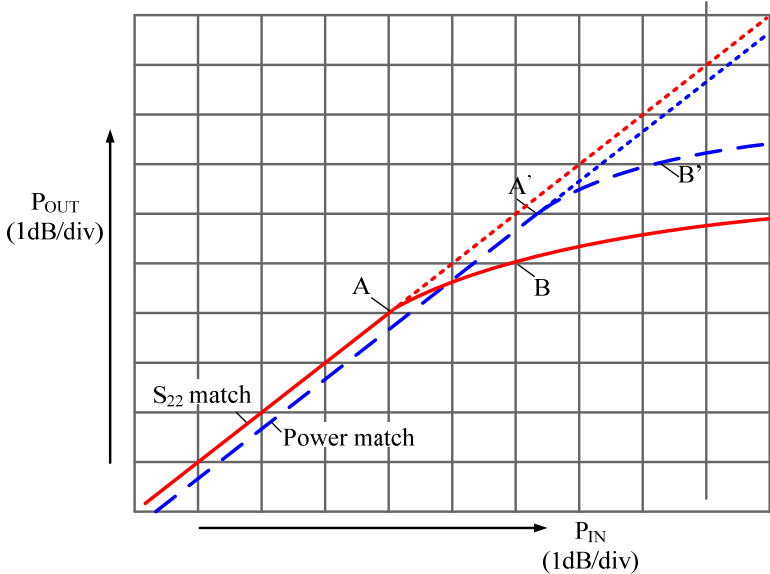


Fig. 2.4. Compression characteristics for conjugate (S_{22}) match (solid curve) and power match (dashed curve). The 1dB compression point (B, B') and maximum linear power point (A, A') show improvements under power-matched conditions.

In a typical situation, the conjugate match would yield a 1 dB compression power significantly lower than that which can be obtained by the correct power tuning, shown by the dashed line in Fig. 2.4. The maximum linear power (A, A') increases with power tuning by about 2 dB as well as the 1 dB compression power (B, B') [11].

2.2 Dual-Band Bias Line

In general, small signal amplifier at UHF uses a chip inductor as the RF choke for bias. The ideal inductors would have zero resistance and zero capacitance. However, the real lumped inductors have the parasitic resistance and capacitance. With those parasitics, the inductor can make a self-resonant frequency (SRF), and it looks like capacitor (negative inductance) at above SRF. So the quarter wavelength ($\lambda/4$) transmission lines, terminated with chip capacitor or radial stubs, are preferred as bias lines in microwave frequencies. Fig. 2.5 shows the conventional $\lambda/4$ bias line. In this figure, the bypass capacitor will short in view of frequency and then $\lambda/4$ transmission line transforms short impedance to the open at point A.

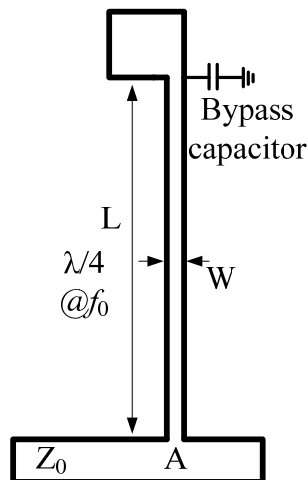


Fig. 2.5. Conventional bias lines.

To minimize the interference between bias and signal transmission lines, the difference between their characteristic impedances should be as large as possible.

Therefore, $\lambda/4$ transmission lines with very high impedance are generally used.

But since the high power transistors consume higher currents, the width of the bias line should be much wider than that of small power transistor to avoid a voltage drop in the bias line.

2.2.1 Dual-Band Bias Line Theory

Usually, the bias transmission line should not effect to the RF signal transmission line at the operate frequencies. Fig. 2.6 shows topology of dual-band bias line. The operation of the dual-band bias line can be explained as follows. Within this topology the input impedance (Z_{in}) is given by equation 2.7.

$$Z_{in} = Z_1 \frac{j[-Z_2 Z_3 \cot(\theta_2) \tan(\theta_3) + Z_3 \tan(\theta_3) Z_1 \tan(\theta_1) - Z_2 \cot(\theta_2) Z_1 \tan(\theta_1)]}{[Z_1 Z_3 \tan(\theta_3) - Z_1 Z_2 \cot(\theta_2) + Z_2 Z_3 \cot(\theta_2) \tan(\theta_3) \tan(\theta_1)]} \quad (2.7)$$

At the second pass band (f_2), the electrical length of transmission line 2 (TL₂) is $\lambda/4$. It transform from open condition to the short impedance at connection point (node A) at f_2 . Again, transmission line 1 (TL₁) is $\lambda/4$ at f_2 and it provides to the open at the connection point B as shown in Fig. 2.3(b). Therefore, there is no effect to the signal TL Z_0 at f_2 .

At the first passband (f_1), the summing impedance of TL₂ and TL₃ is operated as a termination impedance of TL₁. The input impedance Z_{in} at the point B is derived as the equation 2.7. Where the variables Z_1 , Z_2 , θ_1 , and θ_2 , are known. To provide Z_{in} as open (infinite) the denominator of equation 2.7 should be zero, so that θ_3 can

be derived as in equation 2.8

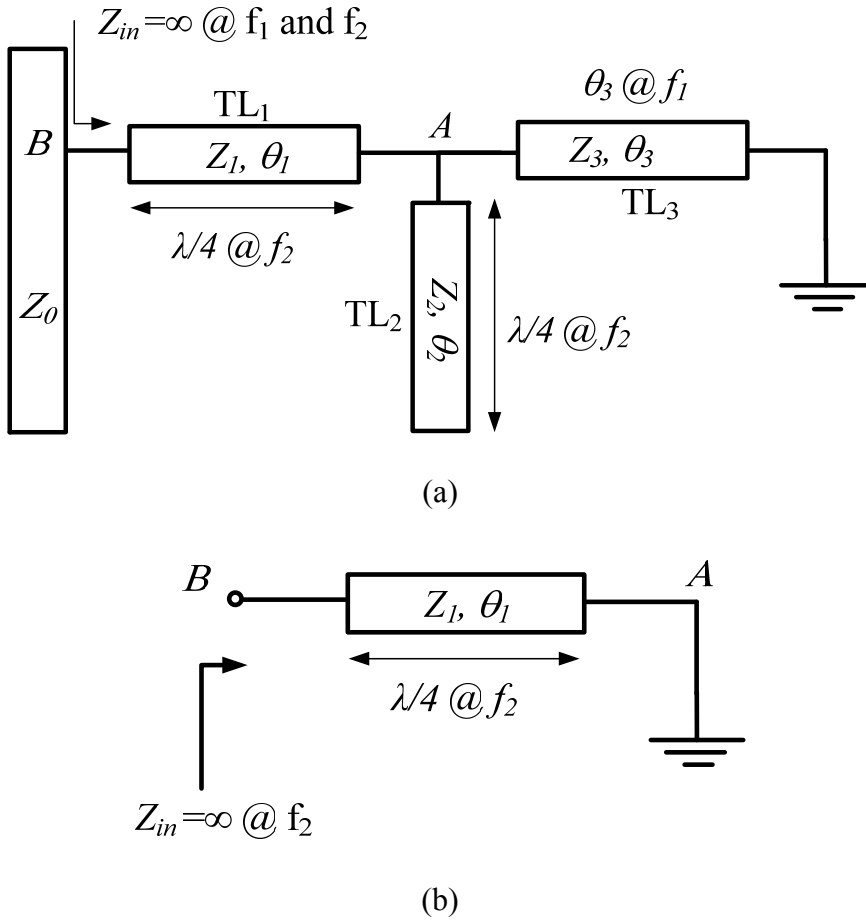


Fig. 2.6. Topology of dual-band bias line: (a) full structure and (b) equivalent circuit at f_2 .

$$\theta_3 = \tan^{-1} \left\{ \frac{Z_1 Z_2 \cot(\theta_2)}{[Z_1 Z_3 + Z_2 Z_3 \cot(\theta_2) \tan(\theta_1)]} \right\} \quad (2.8)$$

The electrical length of θ_3 is depending on f_1 .

2.2.2 Simulations and Measurements

To show a validity of dual-band bias line, two operating frequencies are selected as $f_1=0.881$ GHz and $f_2=2.14$ GHz. In this work RT/Duriod 5880 of Rogers with 2.2 of dielectric constant (ϵ_r) and 31mils (0.787mm) of thickness (h) is used. By given the characteristic impedance $Z_1=Z_2=Z_3=120 \Omega$, the electrical length of θ_3 is 33.52 degree at f_1 . Fig. 2.7 shows the layout of dual-band bias line printed on RT/Duriod 5880.

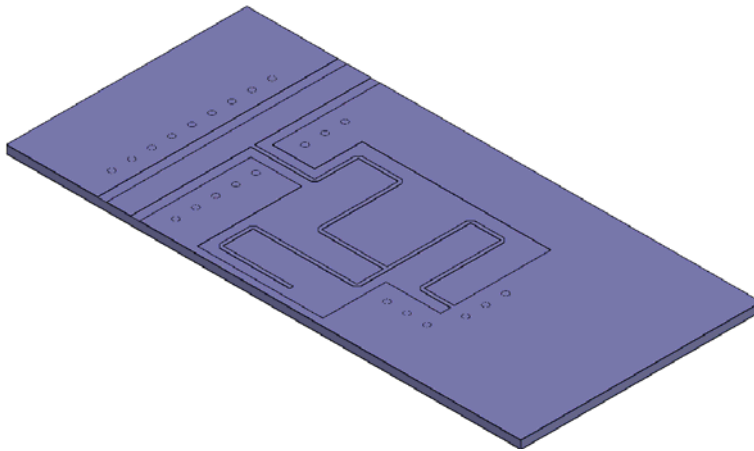
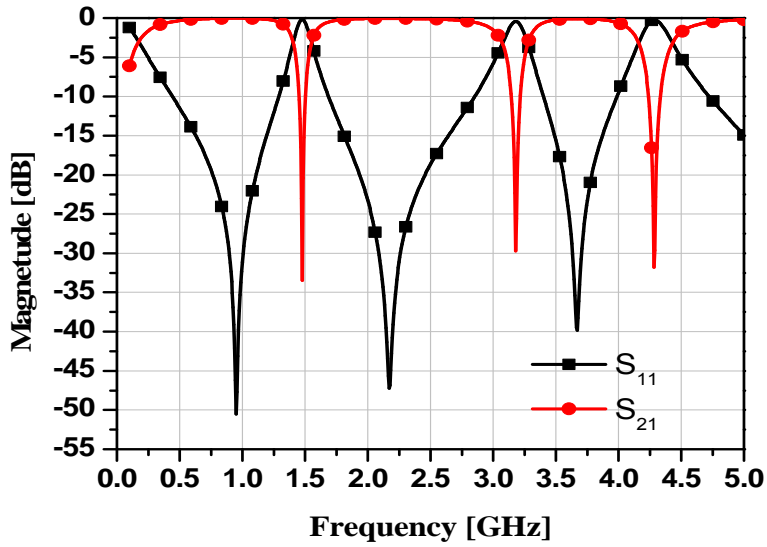
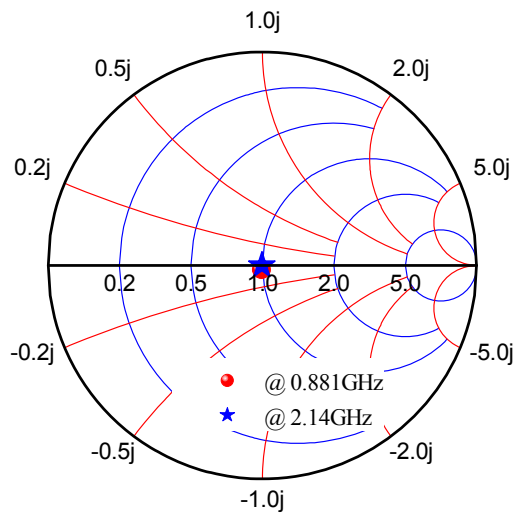


Fig. 2.7. Layout of dual_band bias line.

The EM simulation result of dual-band bias line of Fig. 2.7 using EM simulator HFSS of Ansoft is shown in Fig. 2.8. Moreover, Fig. 2.8(a) shows the EM simulation result of the insertion loss and return loss characteristic of dual-band bias line. The return loss of both bands is below 33 dB where the insertion loss is almost Zeros. Fig. 2.8(b), the operate frequencies are present at the middle of smith chart. It means this dual-band bias line is not affected to the feed line (Z_0).



(a)



(b)

Fig 2.8 EM simulation result of dual-band bias line: (a) amplitude of S_{11}/S_{21} characteristic and (b) impedance characteristic.

Fig. 2.9 shows the photograph of the fabricated dual-band bias line. The measurement of magnitude (S_{11} and S_{21}) and impedance characteristic are shown in Fig. 2.10(a) and 2.10(b), respectively.

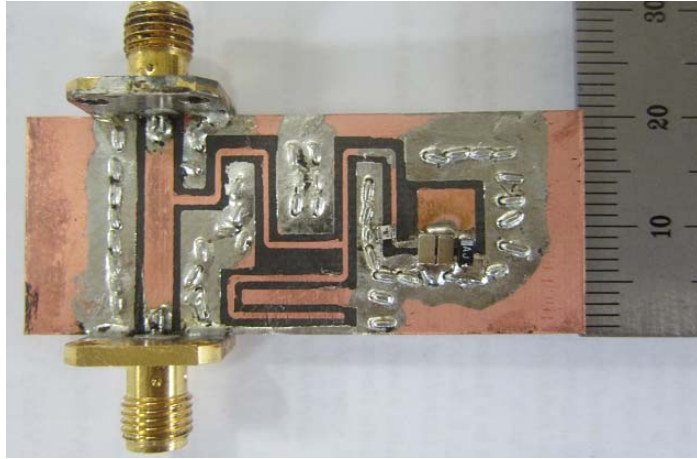
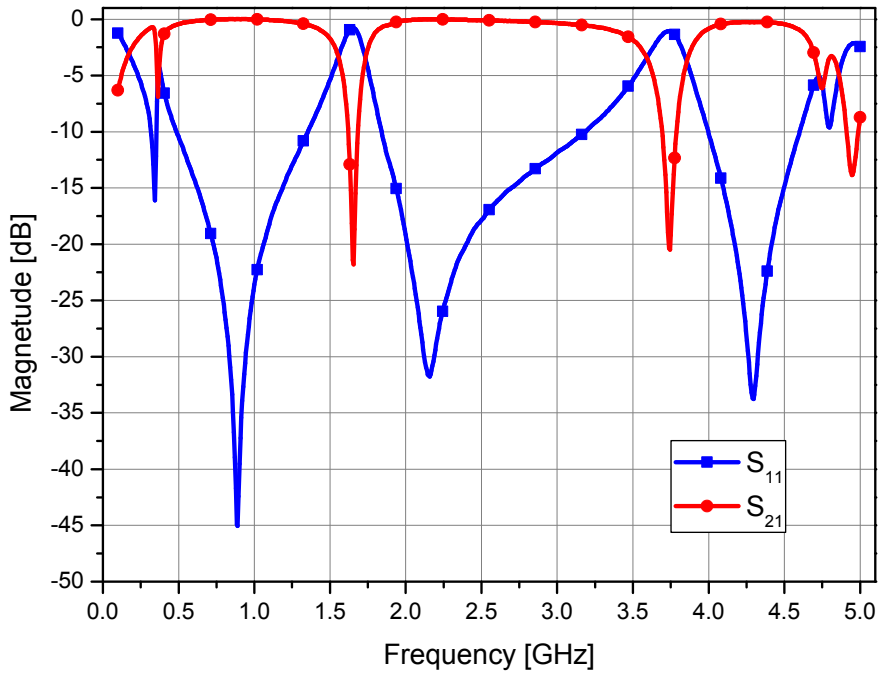
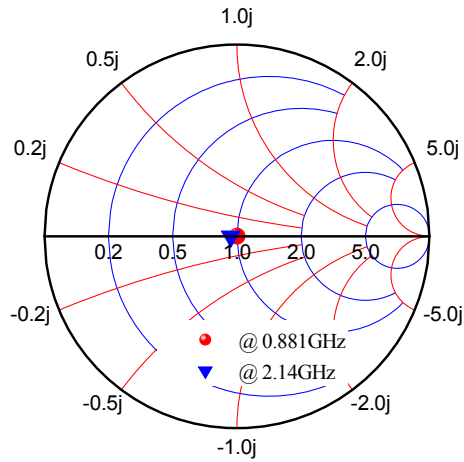


Fig. 2.9. The photograph of proposed dual-band bias line.



(a)



(b)

Fig. 2.10. The measurement result of proposed dual-band bias line: (a) insertion loss and return loss (S_{21} , S_{11}) and (b) impedance characteristic.

2.3 Realized Inductor with High Impedance Transmission Line

The lumped circuit elements are usually unattainable at microwave frequencies, so that the distributed elements are more commonly used [12]. Also, the lumped elements such as inductors are generally available only for a limited range of values and low quality factors (Q). In this work, a high impedance transmission line is used instead of lumped inductor.

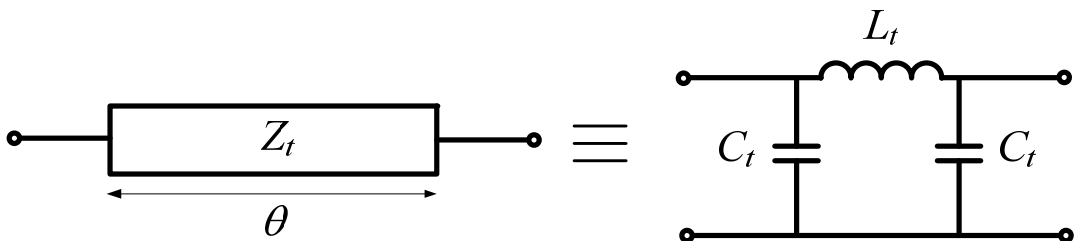


Fig. 2.11. Transmission line and a lumped elements equivalent circuit.

The equivalent lumped network can be derived using ABCD parameter of transmission line and lumped element equivalent circuit [13]. Fig. 2.11 shows a transmission line and a lumped elements equivalent circuit. Equation (2.9) and (2.10) are the ABCD matrix of transmission line and equivalent circuit, respectively. By comparing ABCD matrix of (2.9) and (2.10), the equivalent lumped elements can be derived as (2.11) and (2.12).

$$\begin{bmatrix} A & B \\ C & D \end{bmatrix} = \begin{bmatrix} \cos \theta_t & jZ_t \sin \theta_t \\ j\frac{\sin \theta_t}{Z_t} & \cos \theta_t \end{bmatrix} \quad (2.9)$$

$$\begin{aligned} \begin{bmatrix} A & B \\ C & D \end{bmatrix} &= \begin{bmatrix} 1 & 0 \\ j\omega C_t & 1 \end{bmatrix} \begin{bmatrix} 1 & j\omega L_t \\ 0 & 1 \end{bmatrix} \begin{bmatrix} 1 & 0 \\ j\omega C_t & 1 \end{bmatrix} \\ &= \begin{bmatrix} 1 - \omega^2 L_t C_t & j\omega L_t \\ j\omega(2C_t - \omega^2 L_t C_t^2) & 1 - \omega^2 C_t L_t \end{bmatrix} \end{aligned} \quad (2.10)$$

$$L_t = \frac{Z_t \sin \theta_t}{\omega} \quad (2.11)$$

$$C_t = \frac{1 - \cos \theta_t}{\omega Z_t \sin \theta_t} \quad (2.12)$$

CHAPTER 3 DESIGN OF DUAL-BAND IMPEDANCE MATCHING NETWORK

This chapter, a designing of dual-band matching network is analyzed with theoretical analysis. The transmission zero can be occurred the out-of-band due to the LC resonators. The design theory and some condition to design dual-band matching network will be described the following subsection.

3.1 Design Theory

The impedance transformers or matching networks are a basic design issue in RF circuit and systems. The primary function of impedance matching is to reduce reflection between two connected circuits and allow the maximum power delivery to the load. The common matching network is only used to match the impedance between two circuit elements at the operating center frequency and rarely consider an out-band suppression characteristics. However, in this work the proposed dual-band matching network is realized with three resonators. There are two steps to be realized the proposed dual-band matching network. First of all, a T-type single band matching network is designed at two operating frequencies shown in Fig. 3.1(a) and 3.1(b). Each arm of T-type single band matching network can be realized with the inductor or capacitor. Although a simple L-type matching network is used generally, the T-type matching network is adopted for the out-of-band attenuation characteristics. A pi-type matching network can be used as another

shape of T-type.

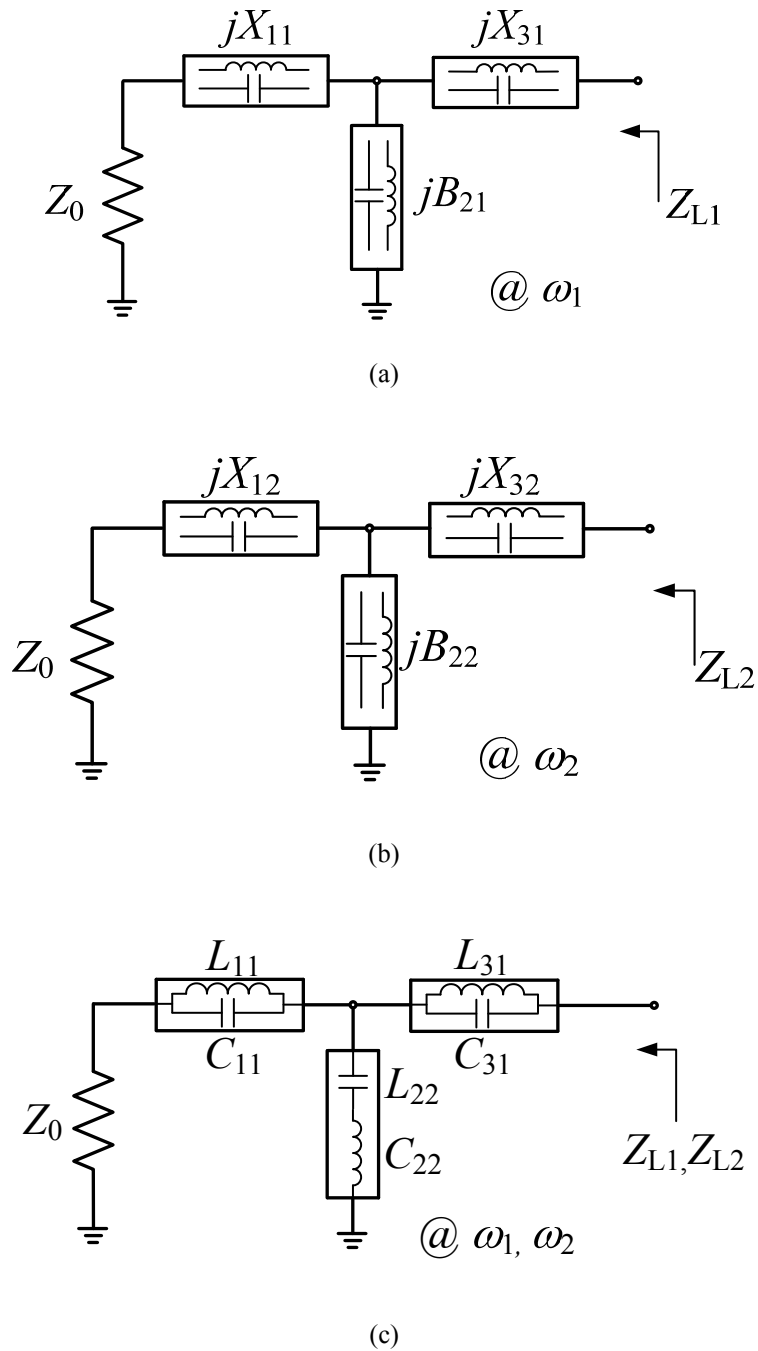
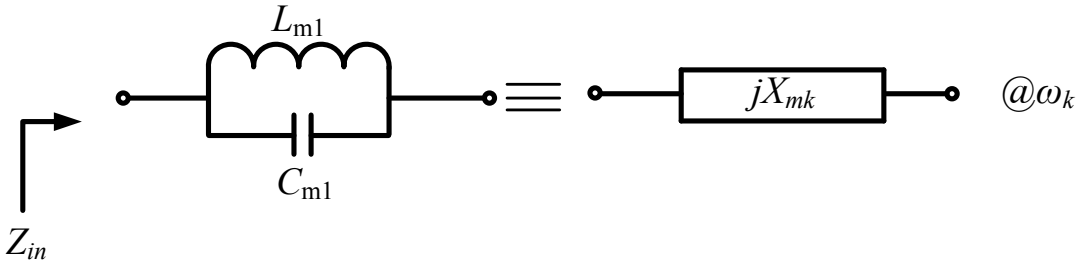


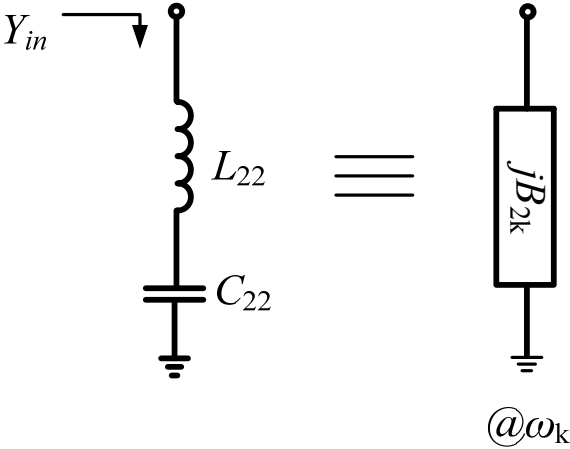
Fig. 3.1. The combination of dual-band matching networks: (a) single band matching network at first band, (b) single band matching network at second band, and (c) Dual-band matching network.

Second, two single band matching networks can be converted into the dual-band matching network using the reactance and susceptance of single band matching network shown in Fig. 3.1(c).

3.1.1 Derivation of Inductance and Capacitance in Dual-Band matching



(a)



(b)

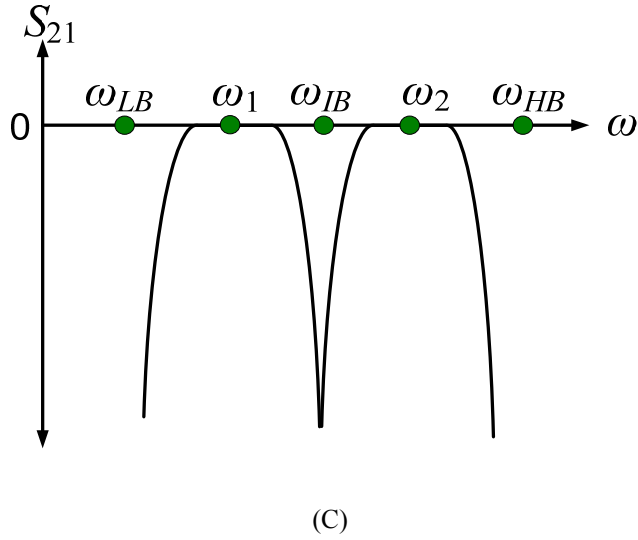


Fig. 3.2. Characteristics of LC resonators and transmission zeros: (a) series-parallel resonator ($m=1$ or 3), (b) shunt-series resonator, and (c) transmission zero characteristic.

The inductance and capacitance of dual-band matching network are obtained from reactances and susceptance of both single band T-type matching networks. Fig. 3.2 (a) shows the parallel LC and equivalent reactance (X_{mk}) of dual-band matching network. The input impedance of parallel LC equal to the reactance (X_{mk}) is given by (3.1).

$$Z_{in} = \frac{j\omega_k L_{m1}}{1 - \omega_k^2 L_{m1} C_{m1}} = jX_{mk} \quad (3.1)$$

Applying ($k=1$ and 2) to equation (3.1), the capacitance and inductance of series-parallel LC is given by (3.2) and (3.3), respectively. ω_k is the operating frequency bands.

$$C_{m1} = \frac{X_{m2}\omega_1 - X_{m1}\omega_2}{X_{m1}X_{m2}(\omega_2^2 - \omega_1^2)}, \quad m = 1, 3 \quad (3.2)$$

$$L_{m1} = \frac{X_{m1}X_{m2}(\omega_2^2 - \omega_1^2)}{\omega_1\omega_2(X_{m2}\omega_2 - X_{m1}\omega_1)}, \quad m = 1, 3 \quad (3.3)$$

Where X_{m1} , X_{m2} , ω_1 , and ω_2 are the reactance of L or C at the first-band, at the second-band, the operating frequency at the first-, and at the second-band, respectively. Similarly, Fig. 3.2 (b) shows the shunt-series LC and equivalent susceptance of dual-band matching network. The input admittance (Y_{in}) of shunt-series LC is equal to susceptance B_{2k} given by (3.4).

$$Y_{in} = \frac{j\omega_k C_{22}}{1 - \omega_k^2 L_{22} C_{22}} = jB_{2k} \quad (3.4)$$

Applying ($k=1$ and 2) to equation 3.4, the inductance and capacitance of shunt-series LC is given by (3.5) and (3.6), respectively.

$$L_{22} = \frac{\omega_1 B_{22} - \omega_2 B_{21}}{B_{21} B_{22} (\omega_2^2 - \omega_1^2)} \quad (3.5)$$

$$C_{22} = \frac{B_{21} B_{22} (\omega_2^2 - \omega_1^2)}{\omega_1 \omega_2 (\omega_2 B_{22} - \omega_1 B_{21})} \quad (3.6)$$

B_{21} and B_{22} are the susceptance of the first- and second-band, respectively. Fig.

3.1(c) shows the proposed structure of dual-band matching network which consists of three LC resonators. The proposed dual-band matching network can simultaneously match two operating frequency band impedances, besides it can create three transmission zeros at the out-of-band frequencies as shown in Fig. 3.2(c). These three resonators can be occurred out-of-band frequency such low ω_{LB} , intermediate ω_{IB} and high ω_{HB} bands shown in Fig. 3.2(c).

The characteristics of proposed dual-band matching network can be found by finding the input impedance/admittance of the resonators. The first and the last series-parallel resonator give the input impedance is given by (3.7) as:

$$Z_{in} = \frac{1}{j\omega_i C_{m1} \left(\frac{\omega_k}{\omega_i} - \frac{\omega_i}{\omega_k} \right)} \quad (3.7)$$

Where $\omega_i^2 = 1/L_{m1}C_{m1}$ for series-parallel resonator.

The input admittance of shunt-series resonator can be calculated by (3.8):

$$Y_{in} = \frac{1}{j\omega_i L_{22} \left(\frac{\omega_k}{\omega_i} - \frac{\omega_i}{\omega_k} \right)} \quad (3.8)$$

Where $\omega_i^2 = 1/L_{22}C_{22}$ for shunt-series resonator ($i=LB, IB, HB$). The LB, IB and HB are standing for low, intermediate and high band as shown in Fig. 3.2(c), respectively. ω_i is resonant frequency. Table 3.3 shows the different combinations

of conditions of series-parallel and shunt-series resonator. From this table, it can be proposed dual-band matching network with difference resonator.

3.1.2 Conditions for Inductance and Capacitance

There are some conditions to realize dual-band matching network. These conditions, the inductance and capacitance of series-parallel (LC) of dual-band matching network are depended on reactance of inductor or capacitor of single band matching network. In table 3.1 shows the conditions to get L and C value for series-parallel LC network. The operating frequency ω_2 must be always higher than ω_1 . From the conditions shown in table 3.1, the reactance of second band is always higher than reactance at the first band to provide C_{m1} and L_{m1} are always positive.

TABLE 3.1: CONDITION OF SERIES-PARALLEL LC

$C_{m1} = \frac{X_{m2}\omega_1 - X_{m1}\omega_2}{X_{m1}X_{m2}(\omega_2^2 - \omega_1^2)}, \quad m = 1, 3 \quad (3)$		$L_{m1} = \frac{X_{m1}X_{m2}(\omega_2^2 - \omega_1^2)}{\omega_1\omega_2(X_{m2}\omega_2 - X_{m1}\omega_1)}, \quad m = 1, 3 \quad (4)$	
<p>1) $X_{m1} > 0, X_{m2} > 0$:</p> $\omega_2 X_{m2} - \omega_1 X_{m1} > 0 \rightarrow X_{m2} > \frac{\omega_1}{\omega_2} X_{m1}$ $\omega_1 X_{m2} - \omega_2 X_{m1} > 0 \rightarrow X_{m2} > \frac{\omega_2}{\omega_1} X_{m1}$		$\therefore X_{m2} > \frac{\omega_2}{\omega_1} X_{m1} \quad \frac{X_{m2}}{\omega_2} > \frac{X_{m1}}{\omega_1}$ $\frac{\omega_2 L_2}{\omega_2} > \frac{\omega_1 L_1}{\omega_1} \quad \therefore L_1 < L_2$ <p>L_1, L_2 are inductance of series arm of single band M/N</p> $\therefore 0 < X_{m1} < X_{m2}$	
<p>2) $X_{m1} < 0, X_{m2} < 0$</p> $\omega_2 X_{m2} - \omega_1 X_{m1} > 0 \rightarrow X_{m2} > \frac{\omega_1}{\omega_2} X_{m1}$ $\omega_1 X_{m2} - \omega_2 X_{m1} > 0 \rightarrow X_{m2} > \frac{\omega_2}{\omega_1} X_{m1}$		$\therefore X_{m2} > \frac{\omega_1}{\omega_2} X_{m1} \quad \frac{-\omega_2}{\omega_2 C_2} > \frac{-\omega_1}{\omega_1 C_1}$ $\therefore C_1 < C_2$ <p>C_1, C_2 are capacitance of series arm of single band M/N</p> $\therefore X_{m1} < X_{m2} < 0$	
<p>3) $X_{m1} > 0, X_{m2} < 0$</p> $\omega_2 X_{m2} - \omega_1 X_{m1} < 0 \text{ and } \omega_1 X_{m2} - \omega_2 X_{m1} < 0$ $(-) \quad (-) \quad (-) \quad (-)$		<p>It is always positive</p>	

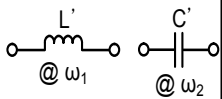
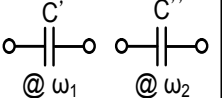
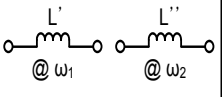
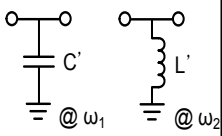
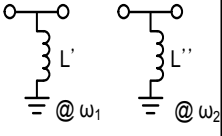
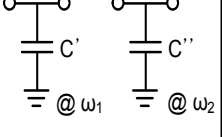
Similarly, the inductance and capacitance of shunt-series (LC) of dual-band matching network are depended on susceptance of inductor or capacitor of single band matching network. In table 3.2 shows the conditions to get L and C value of shunt-series LC network. The operating frequency ω_2 must be always higher than ω_1 . The condition shown in table 3.2, the susceptance of second band is always higher than susceptance at the first band to provide C_{22} and L_{22} are always positive.

TABLE 3.2: CONDITION OF SHUNT-SERIES LC

$L_{22} = \frac{\omega_1 B_{22} - \omega_2 B_{21}}{B_{21} B_{22} (\omega_2^2 - \omega_1^2)} \quad (5)$	$C_{22} = \frac{B_{21} B_{22} (\omega_2^2 - \omega_1^2)}{\omega_1 \omega_2 (\omega_2 B_{22} - \omega_1 B_{21})} \quad (6)$
<p>1) $B_{21} > 0, B_{22} > 0$:</p> $\omega_1 B_{22} - \omega_2 B_{21} > 0 \rightarrow B_{22} > \frac{\omega_2}{\omega_1} B_{21}$ $\omega_2 B_{22} - \omega_1 B_{21} > 0 \rightarrow B_{22} > \frac{\omega_1}{\omega_2} B_{21}$	$\therefore B_{22} > \frac{\omega_2}{\omega_1} B_{21} \quad \frac{\omega_2 C_{s2}}{\omega_2} > \frac{\omega_1 C_{s1}}{\omega_1}$ $C_{s1} < C_{s2}$ $\therefore 0 < B_{21} < B_{22}$ <p style="text-align: right; font-size: small;">C_{s1}, C_{s2} are capacitance of shunt circuit of single band M/N</p>
<p>2) $B_{21} < 0, B_{22} < 0$:</p> $\omega_1 B_{22} - \omega_2 B_{21} > 0 \rightarrow B_{22} > \frac{\omega_2}{\omega_1} B_{21}$ $\omega_2 B_{22} - \omega_1 B_{21} > 0 \rightarrow B_{22} > \frac{\omega_1}{\omega_2} B_{21}$	$\therefore B_{22} > \frac{\omega_1}{\omega_2} B_{21} \quad \frac{-\omega_2}{\omega_2 L_{s2}} > \frac{-\omega_1}{\omega_1 L_{s1}}$ $L_{s1} < L_{s2}$ $\therefore B_{21} < B_{22} < 0$ <p style="text-align: right; font-size: small;">L_{s1}, L_{s2} are inductance of shunt circuit of single band M/N</p>
<p>3) $B_{21} > 0, B_{22} < 0$:</p> $\omega_1 B_{22} - \omega_2 B_{21} < 0 \text{ and } \omega_2 B_{22} - \omega_1 B_{21} < 0$ <p style="text-align: center;">(-) (-) (-) (-) It is always positive</p>	

Table 3.3 shows the input impedance and input admittance at each resonance frequencies. The input impedance and input admittance can be inductor or capacitor depending on the sign of denominator of (3.7) and (3.8). The combinations of T-type matching network can choose with a difference or the same resonator to realized dual-band matching network.

TABLE 3.3: ANALYSIS OF LC RESONATOR

	Conditions	Input impedance	Resonance combination
Series-parallel resonator	Case 1: $\omega_i = 2\pi f_{IB} = \omega_{IB}$	$Z_{in} \left \begin{array}{l} \omega_k = \omega_1 \\ \omega_k < \omega_{IB} \end{array} \right. = \frac{1}{j\omega_{IB}C \left(\frac{\omega_1}{\omega_{IB}} - \frac{\omega_{IB}}{\omega_1} \right)} = \frac{1}{-j\omega_{IB}C} = \frac{j}{\omega_{IB}C} = j\omega_{IB}L'$	
		$Z_{in} \left \begin{array}{l} \omega_k = \omega_2 \\ \omega_k > \omega_{IB} \end{array} \right. = \frac{1}{j\omega_{IB}C \left(\frac{\omega_2}{\omega_{IB}} - \frac{\omega_{IB}}{\omega_2} \right)} = \frac{1}{j\omega_{IB}C} = \frac{1}{j\omega_{IB}C'}$	
	Case 2: $\omega_i = 2\pi f_{LB} = \omega_{LB}$	$Z_{in} \left \begin{array}{l} \omega_k = \omega_1 \\ \omega_k > \omega_{LB} \end{array} \right. = \frac{1}{j\omega_{LB}C \left(\frac{\omega_1}{\omega_{LB}} - \frac{\omega_{LB}}{\omega_1} \right)} = \frac{1}{j\omega_{LB}C} = \frac{1}{j\omega_{LB}C'}$	
		$Z_{in} \left \begin{array}{l} \omega_k = \omega_2 \\ \omega_k > \omega_{LB} \end{array} \right. = \frac{1}{j\omega_{LB}C \left(\frac{\omega_2}{\omega_{LB}} - \frac{\omega_{LB}}{\omega_2} \right)} = \frac{1}{j\omega_{LB}C} = \frac{1}{j\omega_{LB}C''}$	
	Case 3: $\omega_i = 2\pi f_{HB} = \omega_{HB}$	$Z_{in} \left \begin{array}{l} \omega_k = \omega_1 \\ \omega_k < \omega_{HB} \end{array} \right. = \frac{1}{j\omega_{HB}C \left(\frac{\omega_1}{\omega_{HB}} - \frac{\omega_{HB}}{\omega_1} \right)} = \frac{1}{-j\omega_{HB}C} = \frac{j}{\omega_{HB}C} = j\omega_{HB}L'$	
		$Z_{in} \left \begin{array}{l} \omega_k = \omega_2 \\ \omega_k < \omega_{HB} \end{array} \right. = \frac{1}{j\omega_{HB}C \left(\frac{\omega_2}{\omega_{HB}} - \frac{\omega_{HB}}{\omega_2} \right)} = \frac{1}{-j\omega_{HB}C} = j\omega_{HB}L''$	
Shunt-series resonator	Case 1: $\omega_i = 2\pi f_{IB} = \omega_{IB}$	$Y_{in} \left \begin{array}{l} \omega_k = \omega_1 \\ \omega_k < \omega_{IB} \end{array} \right. = \frac{1}{j\omega_{IB}L \left(\frac{\omega_1}{\omega_{IB}} - \frac{\omega_{IB}}{\omega_1} \right)} = \frac{1}{-j\omega_{IB}L} = j\omega_{IB}C'$	
		$Y_{in} \left \begin{array}{l} \omega_k = \omega_2 \\ \omega_k > \omega_{IB} \end{array} \right. = \frac{1}{j\omega_{IB}L \left(\frac{\omega_2}{\omega_{IB}} - \frac{\omega_{IB}}{\omega_2} \right)} = \frac{1}{j\omega_{IB}L} = \frac{-j}{\omega_{IB}L'}$	
	Case 2: $\omega_i = 2\pi f_{LB} = \omega_{LB}$	$Y_{in} \left \begin{array}{l} \omega_k = \omega_1 \\ \omega_k > \omega_{LB} \end{array} \right. = \frac{1}{j\omega_{LB}L \left(\frac{\omega_1}{\omega_{LB}} - \frac{\omega_{LB}}{\omega_1} \right)} = \frac{1}{j\omega_{LB}L} = \frac{-j}{\omega_{LB}L'}$	
		$Y_{in} \left \begin{array}{l} \omega_k = \omega_2 \\ \omega_k > \omega_{LB} \end{array} \right. = \frac{1}{j\omega_{LB}L \left(\frac{\omega_2}{\omega_{LB}} - \frac{\omega_{LB}}{\omega_2} \right)} = \frac{1}{j\omega_{LB}L} = \frac{-j}{\omega_{LB}L''}$	
	Case 3: $\omega_i = 2\pi f_{HB} = \omega_{HB}$	$Y_{in} \left \begin{array}{l} \omega_k = \omega_1 \\ \omega_k < \omega_{HB} \end{array} \right. = \frac{1}{j\omega_{HB}L \left(\frac{\omega_1}{\omega_{HB}} - \frac{\omega_{HB}}{\omega_1} \right)} = \frac{1}{-j\omega_{HB}L} = j\omega_{HB}C'$	
		$Y_{in} \left \begin{array}{l} \omega_k = \omega_2 \\ \omega_k < \omega_{HB} \end{array} \right. = \frac{1}{j\omega_{HB}L \left(\frac{\omega_2}{\omega_{HB}} - \frac{\omega_{HB}}{\omega_2} \right)} = \frac{1}{-j\omega_{HB}L} = j\omega_{HB}C''$	

3.1.3 The Combination of T-type Matching Network and Auxiliary combination of T-type Matching Network

There are more than twenty combinations of single band T-type matching network to realize dual-band matching network. Fig. 3.3 shows the six combinations of T-type matching network with a difference out-of-band transmission zeros as IB-LB-HB, LB-HB-IB, HB-IB-LB, and so on. When one of these combinations is occurred the dual-band matching network with transmission zero at the out-of-band can be obtained.

Moreover, the auxiliary combinations of T-type matching network can also be used to design dual-band with out-of-band transmission zero. The combinations can make two transmission zeros present at low-band, intermediate-band, or higher-band by reason of IB-IB-LB, HB-LB-LB, etc. Additionally, the transmission zero can be all occurred at low, intermediate, and higher band on account of IB-IB-IB, LB-LB-LB, and HB-HB-HB combination. Fig. 3.4 shows the auxiliary combination of T-type matching network.

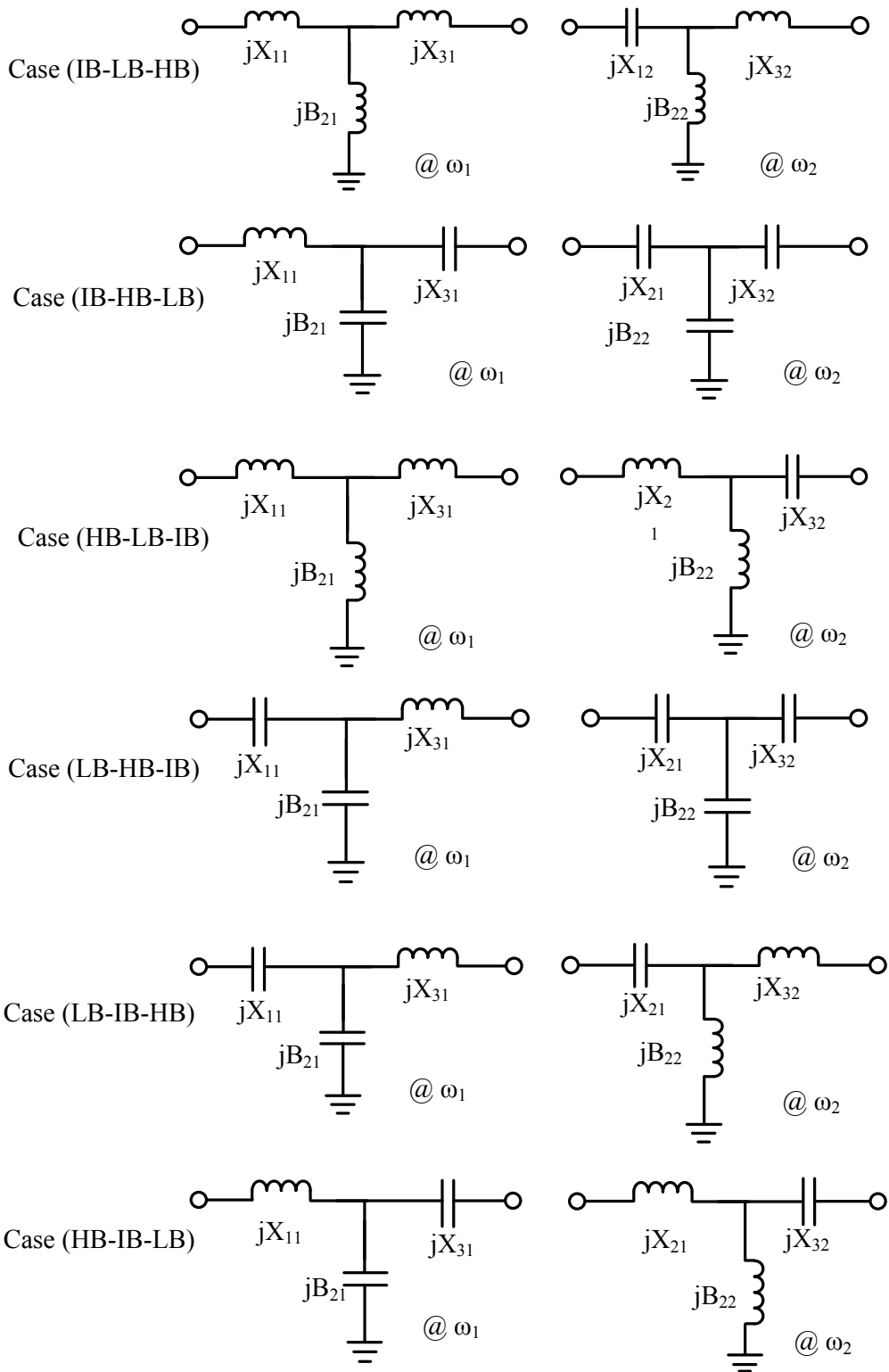


Fig. 3.3. The combinations of T-type matching network.

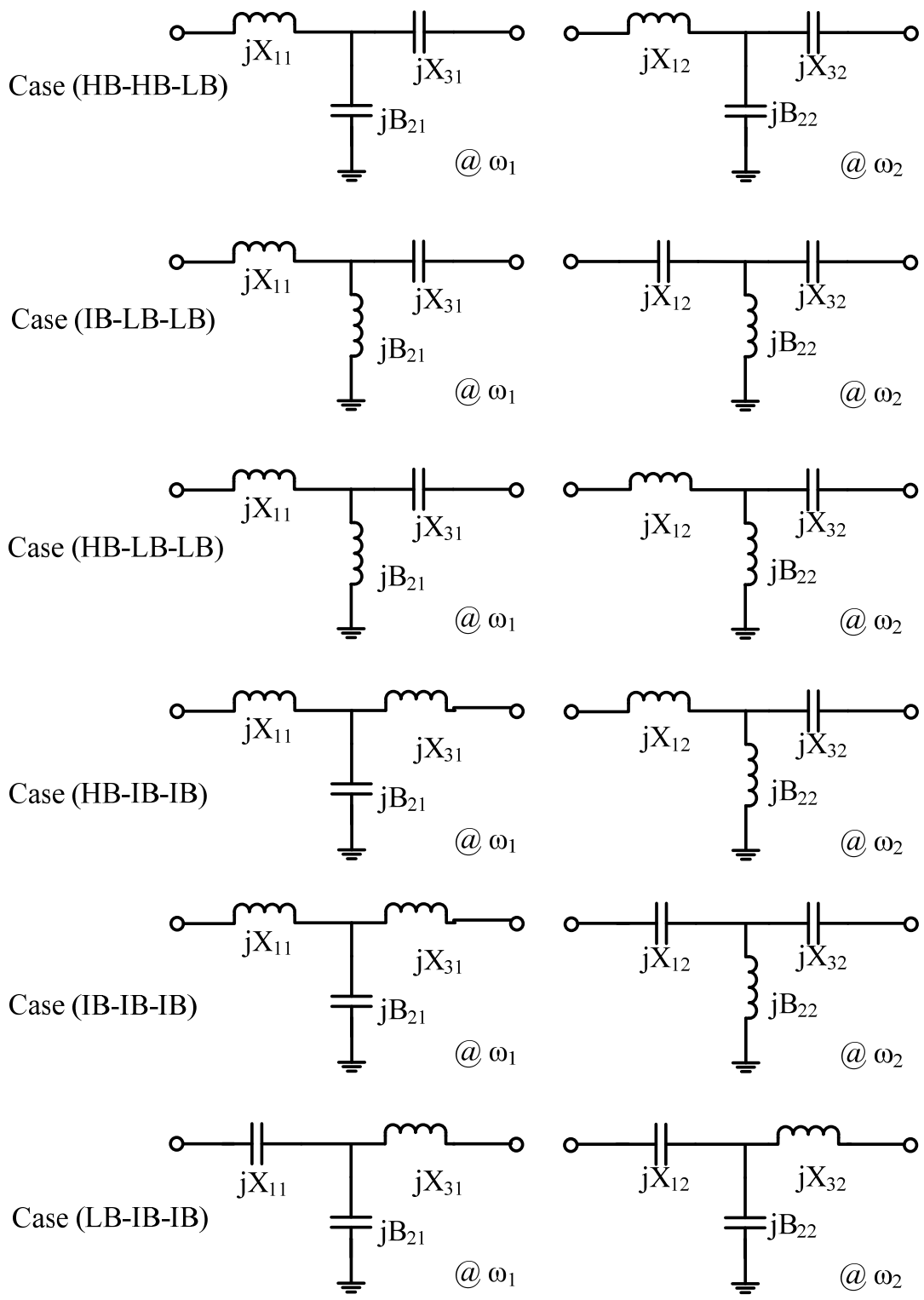


Fig. 3.4. The Auxiliary combination of T-type matching network.

CHAPTER 4 DESIGN OF DUAL-BAND AMPLIFIER WITH OUT-OF-BAND TRANSMISSION ZEROS

ZEROS

In this chapter, the dual-band matching network will be analyzed, simulated, and measured with two operating frequencies of GSM 0.881 GHz and WCDMA 2.14 GHz. And then, using these dual-bands matching at the front-end of amplifier (AH1) to validate the out-off-band transmission zeros. Fig. 4.1 shows the proposed structure of dual-band amplifier with dual-band bias line.

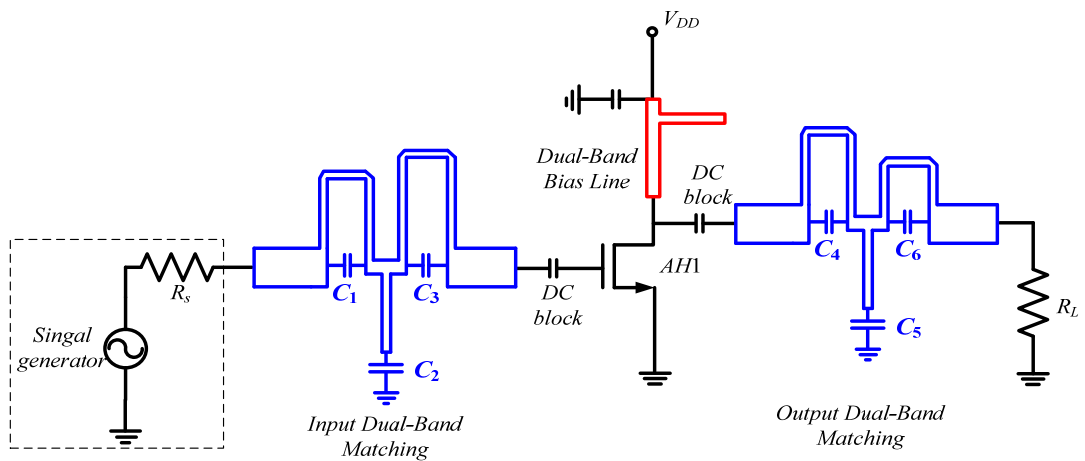


Fig. 4.1. The proposed structure of dual-band amplifier with out-of-band suppression.

4.1 Optimizing the Impedance Matching

In order to design dual-band power amplifier with high output power as well as efficiency, the important parameter is impedance matching should be match at both bands accurately. Fig. 4.2 shows the simplified of load/source pull measurement. First the biasing point of gate and drain, the input power, and the operating

frequency need to be selected. Then the input and output tuner will be adjusted to provide different reflection coefficients at the source side (Γ_{source}) and load side (Γ_{load}) of the transistor. The corresponding output fundamental power and DC power consumption will be measured for each Γ . Since the optimal value of Γ_{load} will depend on the value of Γ_{source} , the process will be repeated several times until optimum performance is achieved. Usually, the optimum PAE (or DE) and the optimum output power will not share the same optimal impedance for load side, and thus the maximum PAE and maximum output power cannot be achieved at the same time. A trade off strategy is needed when selecting the optimum impedance. In addition, the load/source pull technique can be applied to determine optimum impedances at harmonic frequencies. Since the load pull/ source pull technique treats the transistor device as stubs tuning, we loss the insight of the intrinsic voltage and current of the transistor drain and thus have less understanding of the class of operation mode that the transistor is working at. A better solution would be

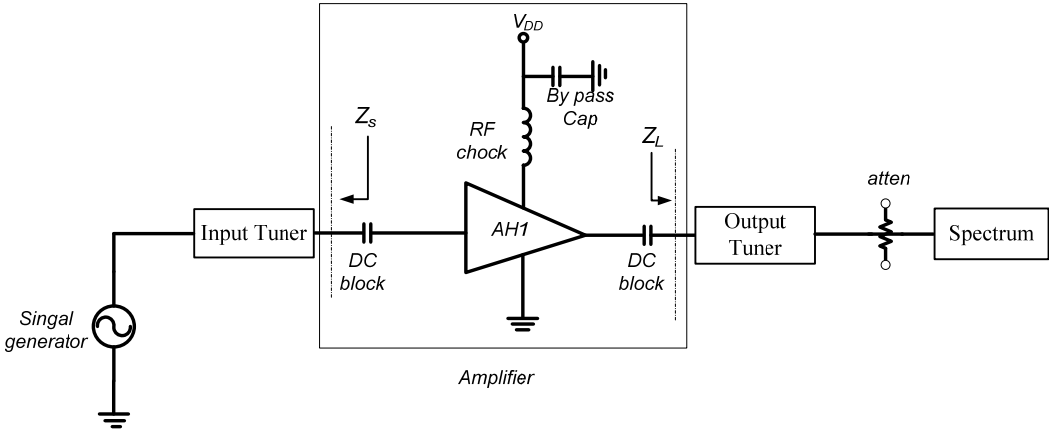
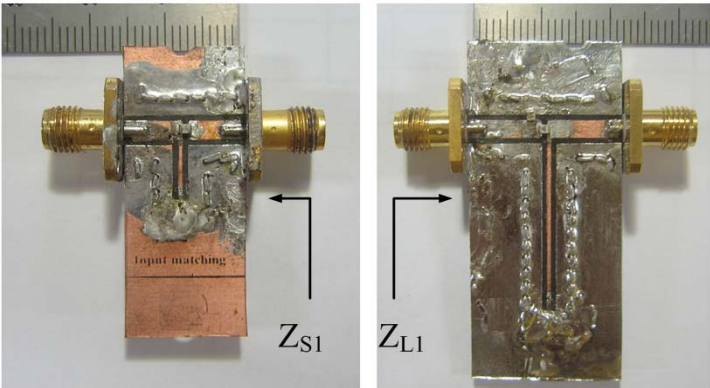


Fig. 4.2. Load/source pull set up.

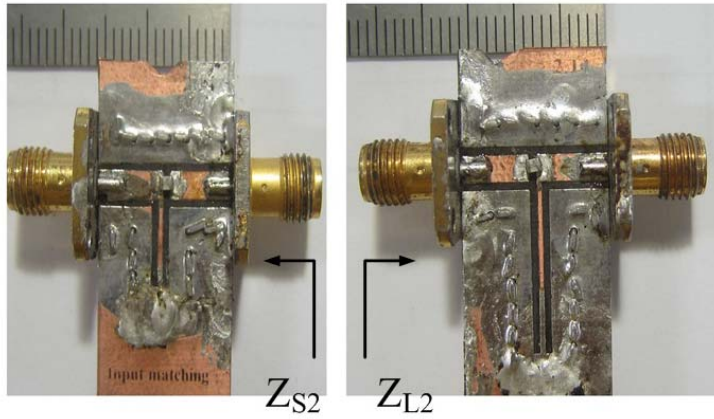
to conduct load pull/source pull and then verify the performance by using single-band matching with real PCB at the individual frequency.

4.1.1 Impedance Matching at 0.881 GHz and 2.14 GHz

The optimizing impedance from the load/source pull measurement is used to design single band matching network to avoid loss inside the tuner. Fig. 4.3 (a) and Fig. 4.3 (b) show the photograph of fabricated PCB of L-type single band matching network at the first band and second band, respectively. The circuits are printed on RT/Duriod 5880 PCB for the given substrate with 2.2 of dielectric constant (ϵ_r) and 31mils (0.787mm) of thickness (h). Fig. 4.4 (a) shows the extracted source impedance (Z_{S1}) $27.829+j28.168 \Omega$ and the load impedance (Z_{L1}) $36.08+j4.412 \Omega$ at first band 0.881 GHz. The source impedance (Z_{S2}) $23.391-j9.4287 \Omega$ and load impedance (Z_{L2}) $39.859-j6.7832 \Omega$ are extracted at the second band 2.14 GHz is shown in Fig. 4.4(b).

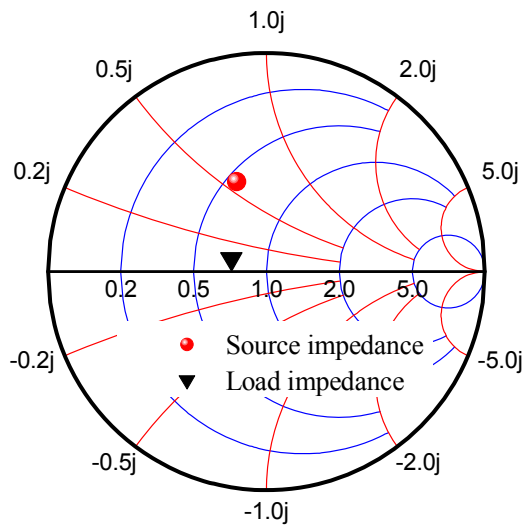


(a)

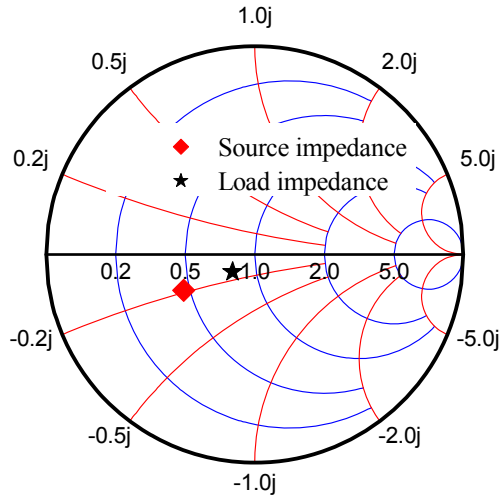


(b)

Fig. 4.3. The fabricated PCB of single band matching networks: (a) at 881 MHz and (b) at 2.14 GHz



(a)



(b)

Fig. 4.4. Extracted impedances: (a) at 0.881GHz and (b) at 2.14GHz.

With these impedances, gain 12.31 dB, output power 22.81 dBm, drain efficiency 37.08 %, and power add efficiency 34.9 % are obtained at 0.881 GHz with drain bias 5 V and drain current 103 mA shown in Fig. 4.5. In this measurement the linear gain is 13.35 dB of output power 3.33 dBm to 20.27 dBm. Also, the trace of PAE and DE are increase while output power increases. The PAE is lower than DE. Fig. 4.6 shows the measured result of gain, PAE, and DE over output power at 2.14 GHz. The linear gain is 11.65 dB of output power 1.72 dBm to 19.66 dBm. The gain at 0.881 GHz is 1.58 dB higher than 2.14 GHz .

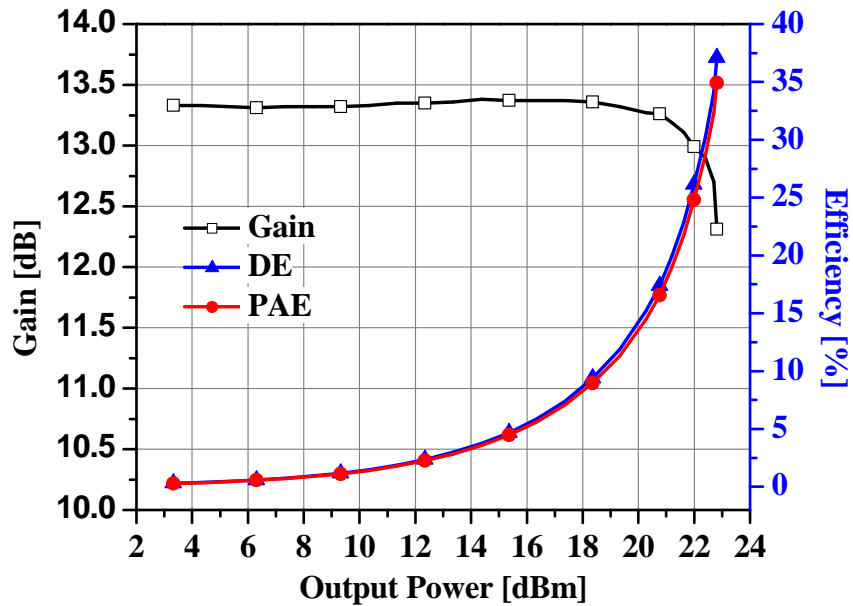


Fig. 4.5. Measured gain and efficiency according to output power at 0.881 GHz.

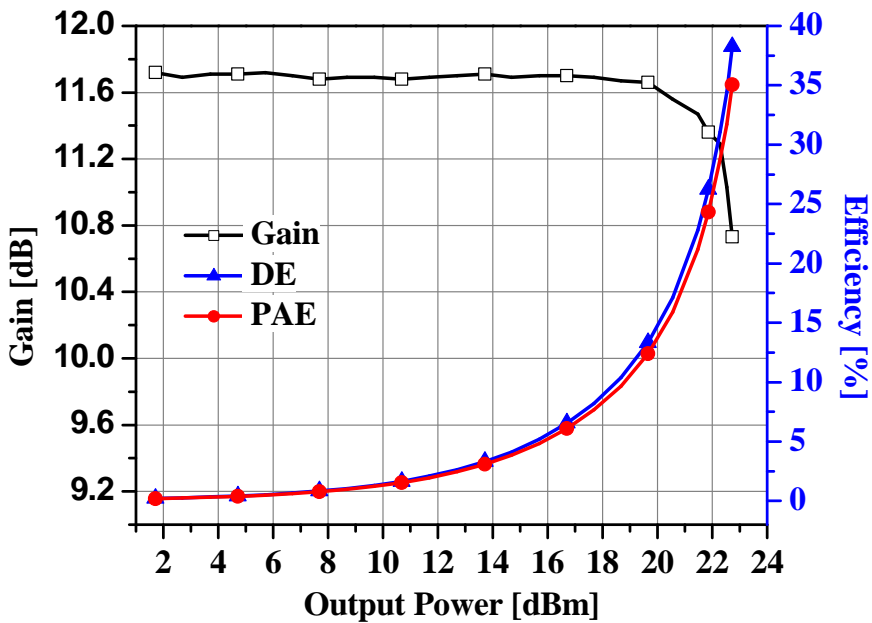


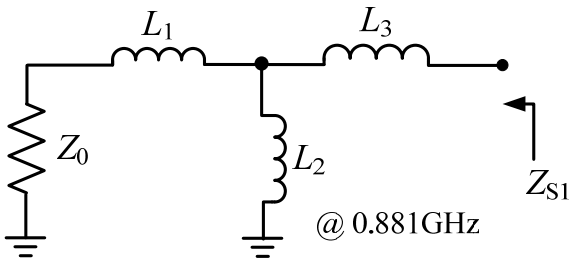
Fig. 4.6. Measured gain and efficiency according to output power at 2.14GHz.

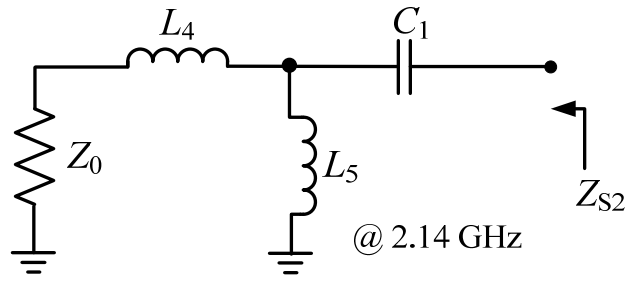
4.2 Realized Input Dual-Band M/N

In the earlier sections, the input and output impedance have been extracted at both bands 0.881 GHz and 2.14 GHz. Base on the above chapter 3 the T-type single band matching network would be designed according to the extracted input and output impedance. The ADS 2009 and HFSS v11 (EM simulation) of Ansoft are used to simulate.

4.2.1 T-type Single Band M/N

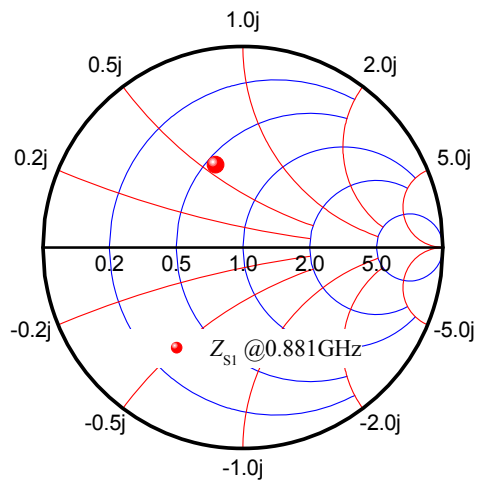
The extracted impedance (Z_{S1}) $27.829+j28.168 \Omega$ and (Z_{S2}) $23.391-j9.4287 \Omega$ at 0.881 GHz and 2.14 GHz, respectively are matched with 50Ω of source impedance. Fig. 4.7 shows the input T-type matching network at 0.881 GHz and 2.14 GHz. Fig. 4.7 (a) shows the input single band matching network at 0.881GHz give the values $L_1= 1.52 \text{ nH}$, $L_2=12.35 \text{ nH}$, and $L_3=0.458 \text{ nH}$. This matching network gives the source impedance (Z_{S1}) $27.836+j28.155 \Omega$ shown in Fig. 4.8(a). Also, Fig. 4.7(b) shows the matching network at second band with elements value $L_4=6.28 \text{ nH}$, $L_5=14.31 \text{ nH}$, and $C_1=1.028 \text{ pF}$. Fig. 4.8 (b) shows the simulation result of source impedance (Z_{S2}) $23.389-j9.376 \Omega$. The simulation result and extracted impedance are well agreed.



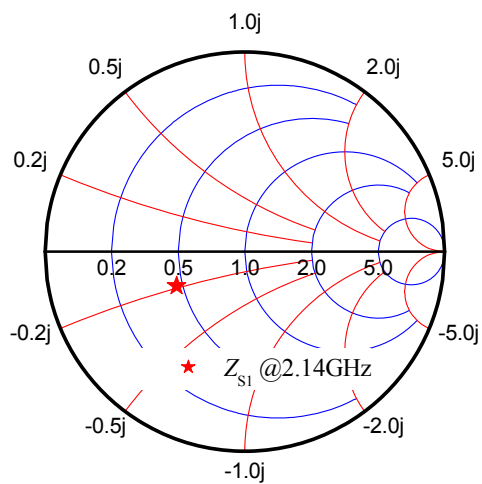


(b)

Fig. 4.7. Input T-type matching networks: (a) at 0.881GHz and (b) at 2.14GHz.



(a)



(b)

Fig. 4.8. Simulation result of source impedances: (a) at 0.881GHz and (b) at 2.14GHz.

4.2.2 Lumped Elements Dual-Band Impedance M/N

The dual-band matching can be realized using reactance and susceptance of T-type matching network in section 4.2.1. Fig. 4.9 shows the input dual-band matching network. The values of series-parallel (L_{S11} , C_{S11}) and (L_{S31} , C_{S31}) are calculated using equation (3.2) and (3.3) the same. The value of shunt-series L_{S22} and C_{S22} are calculated with (3.5) and (3.6), respectively. From the calculation, the value of elements $L_{S11}=1.31$ nH, $C_{S11}=3.321$ pF, $L_{S22}=14.709$ nH, $C_{S22}=13.828$ pF, $L_{S31}=0.3749$ nH, and $C_{S31}=15.77$ pF are obtained. The simulation results are (Z_{S1}) $27.858+j28.144 \Omega$ and (Z_{S2}) $23.704-j11.107 \Omega$ at 0.881GHz and 2.14 GHz, respectively as shown in Fig. 4.10. This result is good agreement between the extracted impedance and simulation result. The structure in Fig. 4.9 all inductors are realized in to transmission line.

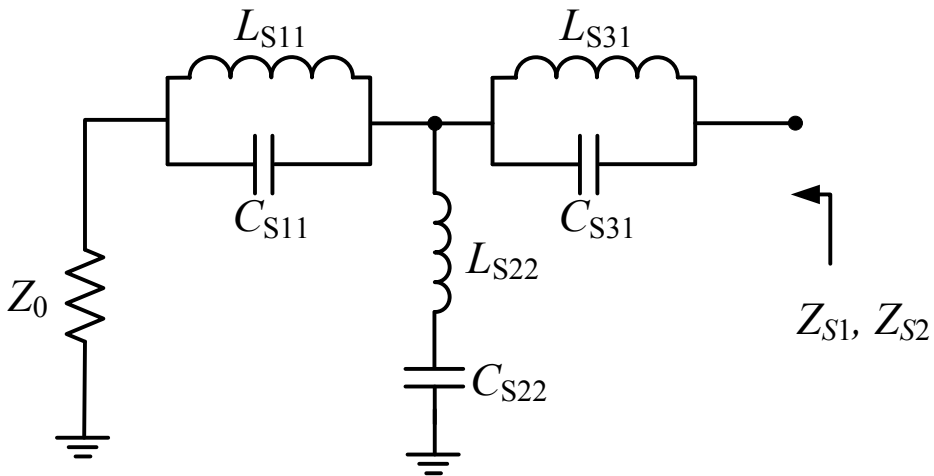


Fig. 4.9. Input dual-band matching network.

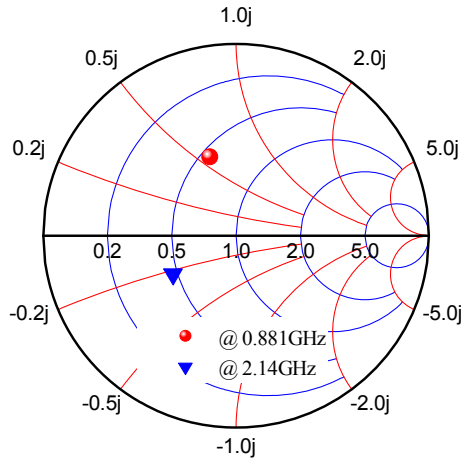


Fig. 4.10. Simulation result of lumped elements input dual-band matching.

4.2.3 Semi-Lumped Elements Dual-Band M/N

The proposed structure is realized inductor to the high impedance transmission line by using equation (2.11). Fig. 4.11 shows the proposed semi-lumped elements dual-band matching.

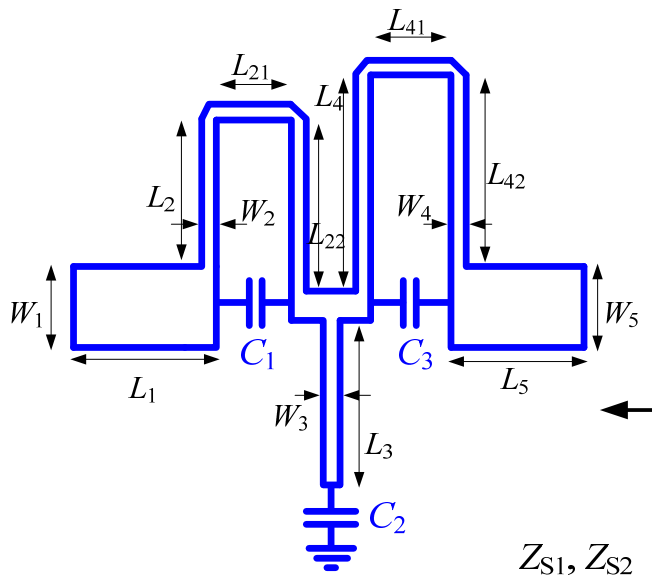


Fig. 4.11. The layout of proposed dual-band matching network.

TABLE 4.1: PHYSICAL LAYOUT OF INPUT DUAL-BAND M/N

Parameters	Physical Length	Unit	Parameters	Physical Length	Unit
$W_1=W_5$	2.4	mm	W_3	0.75	mm
L_1	5	mm	L_4	3.6	mm
L_2	0.85	mm	L_{42}	2.9	mm
$L_{21}=L_{41}$	1	mm	W_4	0.6	mm
L_{22}	1.55	mm	C_1	3.8	pF
W_2	0.35	mm	C_2	15.3	pF
L_3	29	mm	C_3	25	pF
L_5	4	mm			

The physical layouts of proposed dual-band matching network in Fig. 4.11 are shown in table 4.1. The photograph of fabricated PCB is shown in Fig. 4.12. The dual-band matching network is fabricated on the Rogers RT/duroid 5880 substrate with a dielectric constant (ϵ_r) of 2.2 and a thickness (h) of 31 mils.

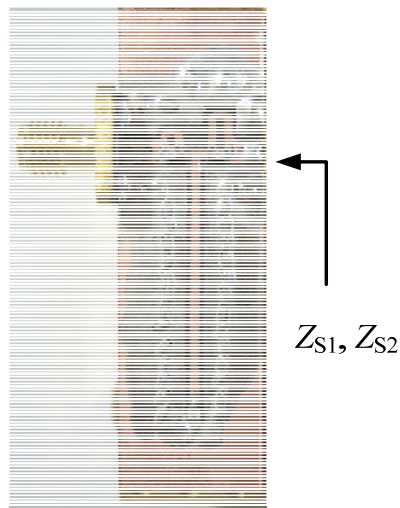


Fig. 4.12. Photograph of fabricated PCB of input dual-band matching network.

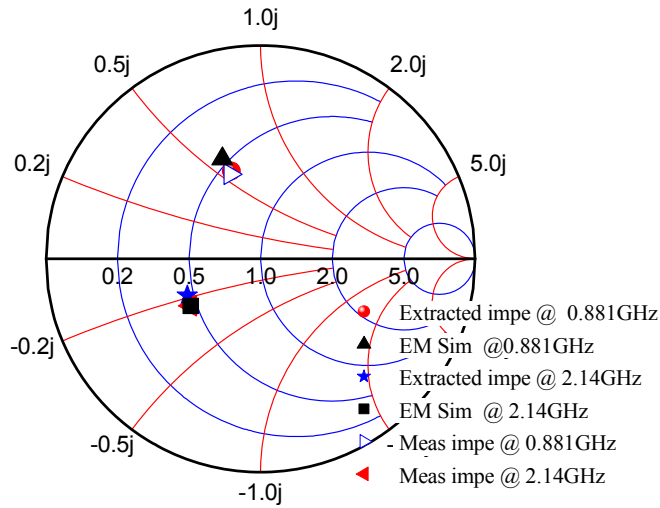


Fig. 4.13. Extracted impedance and measurement impedance of input dual-band matching network.

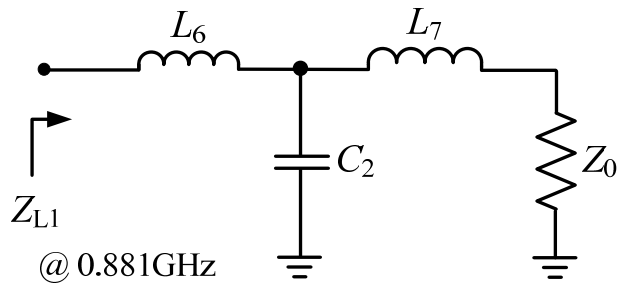
Fig. 4.13 shows the extracted impedance, simulation results, and measurement impedance of input dual-band matching network. The simulation results are $28.2+j29.125 \Omega$ and $24.69-j12.305 \Omega$ at 0.881 GHz and 2.14 GHz, respectively. Moreover, the measurement results are $28.052+j27.081 \Omega$ and $24.515-j12.174 \Omega$ at 0.881 GHz and 2.14 GHz, respectively. The simulation, measurement and extracted result are in good agreement.

4.3 Realized Output Dual-Band M/N

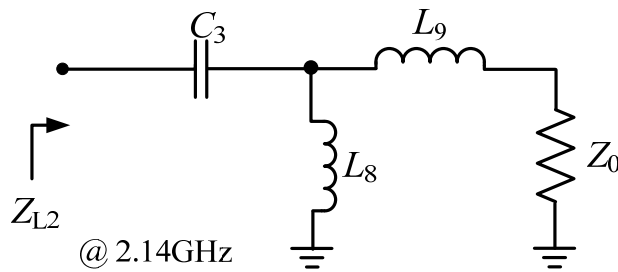
The output dual-band matching network is also following the same procedure as design input dual-band matching network. Likewise, the extracted output impedance (Z_{L1}) $36.08+j4.41 \Omega$ and (Z_{L2}) $39.859-j6.783 \Omega$ at 0.881GHz and 2.14GHz, respectively are matched with 50Ω of load impedance.

4.3.1 T-type Single Band M/N

Fig. 4.14 shows the output T-type matching network at 0.881 GHz and 2.14 GHz. The circuit in Fig. 4.14(a) give the elements value $L_6= 5.02$ nH, $C_2=2.833$ pF, and $L_7=1.4$ nH with the operate frequency 0.881 GHz. The ADS 2009 is used to simulate. This matching network gives the load impedance (Z_{L1}) $36.063+j4.42 \Omega$ shown in Fig. 4.15(a).

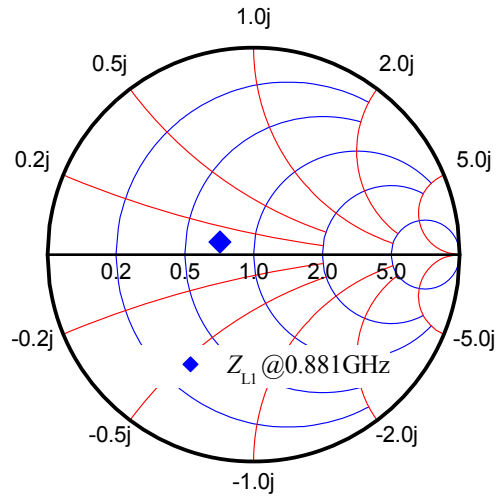


(a)

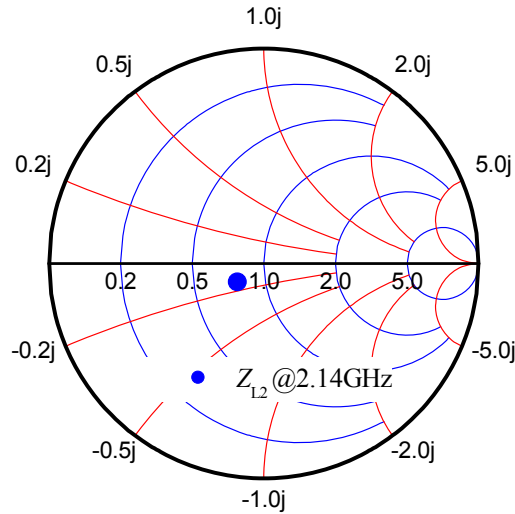


(b)

Fig. 4.14. Output T-type matching networks: (a) at 0.881 GHz and (b) at 2.14 GHz.



(a)



(b)

Fig. 4.15. Simulation results of load impedance: (a) at 0.881GHz and (b) at 2.14GHz.

Also, Fig. 4.14(b) shows the matching network at the second band with elements value $C_3=2.198$ pF, $L_8=13.7$ nH, and $L_9=1.45$ nH. The simulation result is (Z_{L2}) $38.564-j6.74 \Omega$ shown in Fig. 4.15(b). The simulation result and extracted impedance are well agreed.

4.3.2 Lumped Elements Dual-Band Impedance M/N

The dual-band matching is realized using reactance and susceptance of T-type matching network in section 4.2.1. Fig. 4.16 shows the output of lumped element dual-band matching network. The values of series-parallel (L_{L11} , C_{L11}) and (L_{L31} , C_{L31}) are calculated using equation (3.2) and (3.3) the same. And the values of shunt-series L_{L22} and C_{L22} are calculated with (3.5) and (3.6), respectively. From the calculation, the value of elements $L_{L11}=3.115$ nH, $C_{L11}=3.973$ pF, $L_{L22}=18.84$ nH, $C_{L22}=1.07$ pF, $L_{L31}=1.39$ nH, and $C_{L31}=0.164$ pF are obtained. The simulation results are $36.38+j4.556 \Omega$ and $38.541-j6.743 \Omega$ at 0.881 GHz and 2.14 GHz, respectively shown in Fig. 4.17.

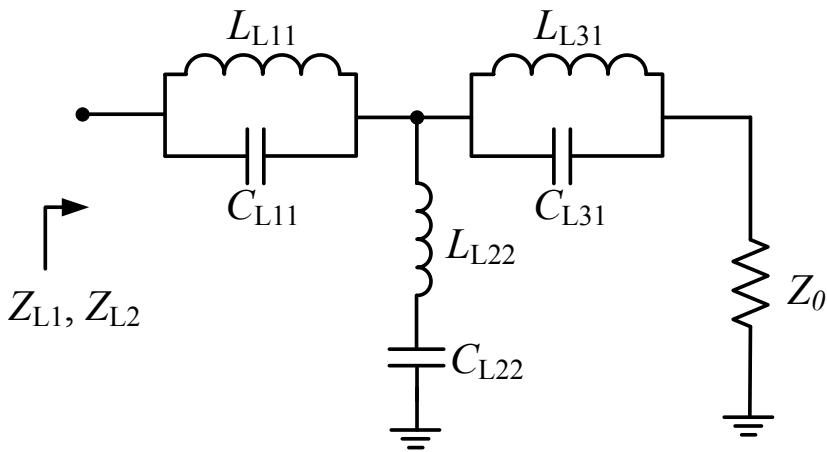


Fig. 4.16. Output lumped elements dual-band matching network.

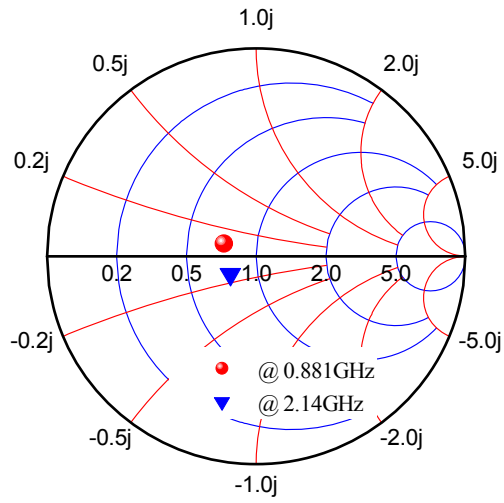


Fig. 4.17. Simulation result of output lumped elements dual-band matching.

4.3.3 Semi-Lumped Elements Dual-Band Impedance M/N

Fig. 4.18 shows the proposed semi-lumped element dual-band matching network.

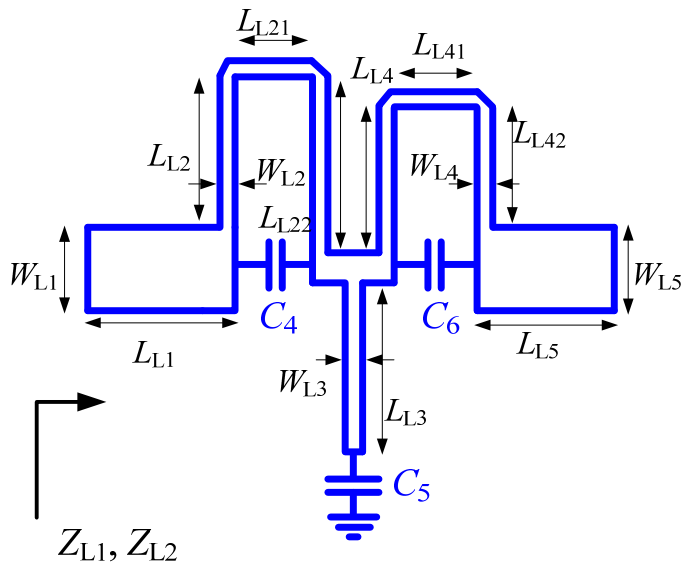


Fig. 4.18. Layout of output dual-band matching network.

TABLE 4.2: PHYSICAL LAYOUT OF OUTPUT DUAL-BAND M/N

Parameters	Physical Length	Unit	Parameters	Physical Length	Unit
$W_{L1}=W_{L5}$	2.4	mm	W_{L3}	0.34	mm
L_{L1}	10	mm	L_{L4}	2.3	mm
L_{L2}	2.25	mm	L_{L42}	1.6	mm
$L_{L21}=L_{L41}$	1	mm	W_{L4}	0.6	mm
L_{L22}	2.95	mm	C_4	2.7	pF
W_{L2}	0.4	mm	C_5	0.38	pF
L_{L3}	37	mm	C_6	0.5	pF
L_{L5}	5	mm			

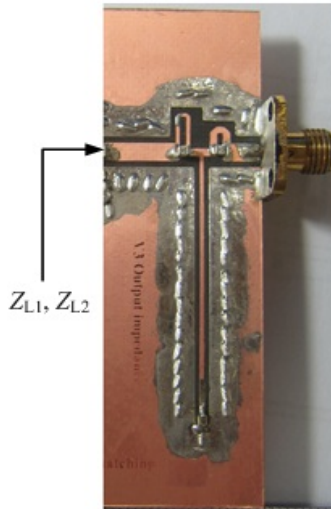


Fig. 4.19. The photograph of fabricated output dual-band matching network.

The inductors of proposed structure are realized to high impedance transmission line by using equation (2.11). The physical layout of dual-band matching network in Fig. 4.18 is mentioned in table 4.2. The photograph of the fabricated PCB is shown in Fig. 4.19. The dual-band matching network is fabricated on the Rogers RT/duroid 5880 substrate.

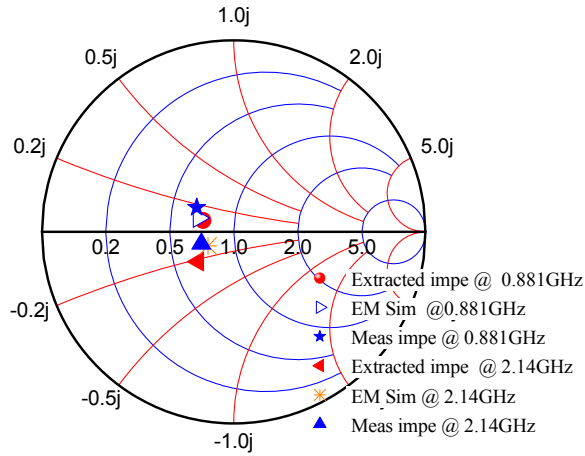


Fig. 4.20. The Extracted impedance, simulation and measurement impedance of input dual-band matching.

Fig. 4.20 shows the extracted impedance, simulation result, and measurement impedance of output dual-band matching network. The simulation results are $34.13 + j5.12 \Omega$ and $37.88 - j5.62 \Omega$ at 0.881GHz and 2.14GHz, respectively. Moreover, the measurement results are $32.9 + j8.88 \Omega$ and $35.344 - j4.61 \Omega$ at 0.881GHz and 2.14GHz, respectively. The results of simulation, measurement and extracted impedance are in good agreement.

4.4 Dual-Band Amplifier

In this subsection, a dual-band amplifier with out-of-band transmission zeros is proposed and experimentally validated. Fig. 4.21 shows the block diagram of the proposed dual-band amplifier which consists of input and output front end of amplifier with chip inductor to feed DC current. And Fig. 4.22 shows the structure of the block diagram of the proposed dual-band amplifier which consists of input

and output front end of the amplifier with dual-band bias transmission line. These topologies can make transmission zeros out-of-bands the same. However, the dual-band amplifier using dual-band bias transmission line can improved attenuation out-of-band.

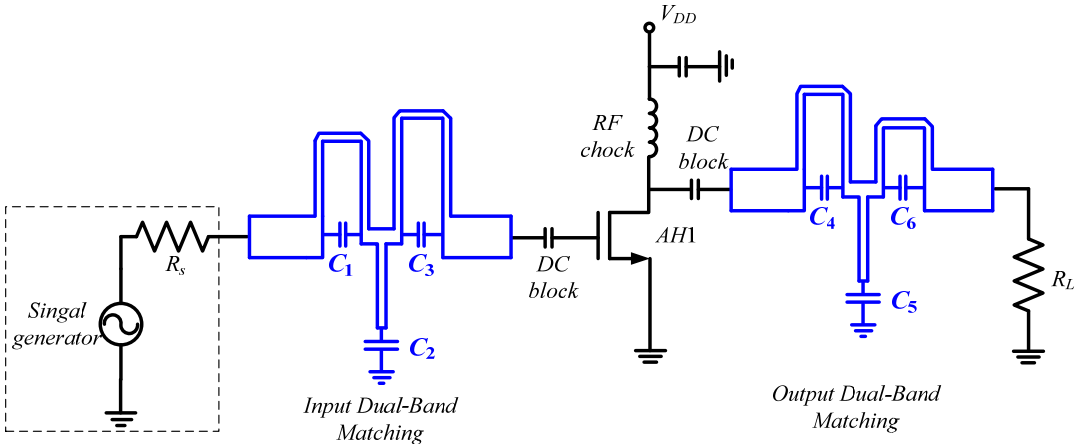


Fig. 4.21. Structure of dual-band amplifier with chip inductor DC bias.

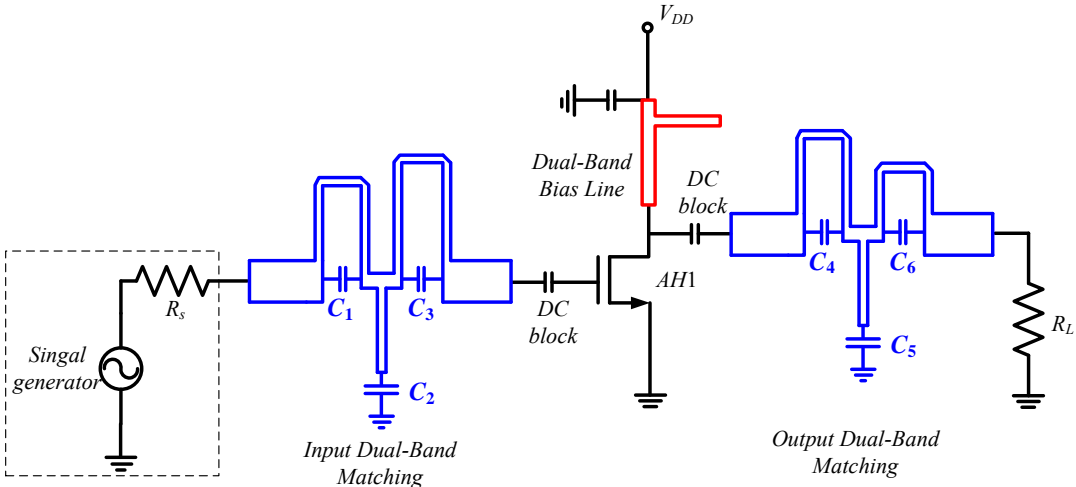


Fig. 4.22. The proposed structure of dual-band amplifier with dual-band bias line.

The amplifier is used High Dynamic Rang Amplifier AH1 with specification of frequency rang from 250 MHz to 3 GHz and can gain up to 13.5 dB with 21 dBm maximum output power.

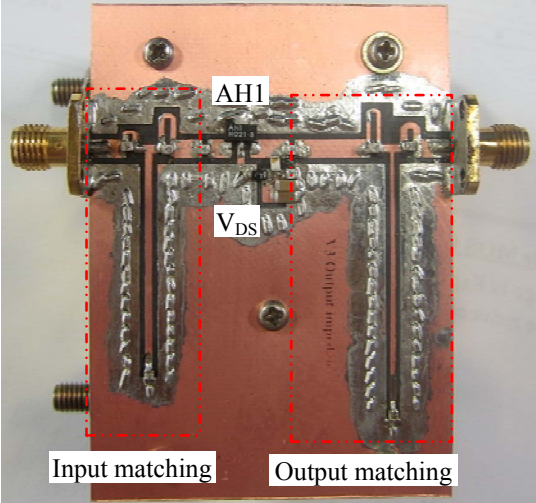


Fig. 4.23. Photograph of the dual-band amplifier with bias inductor.

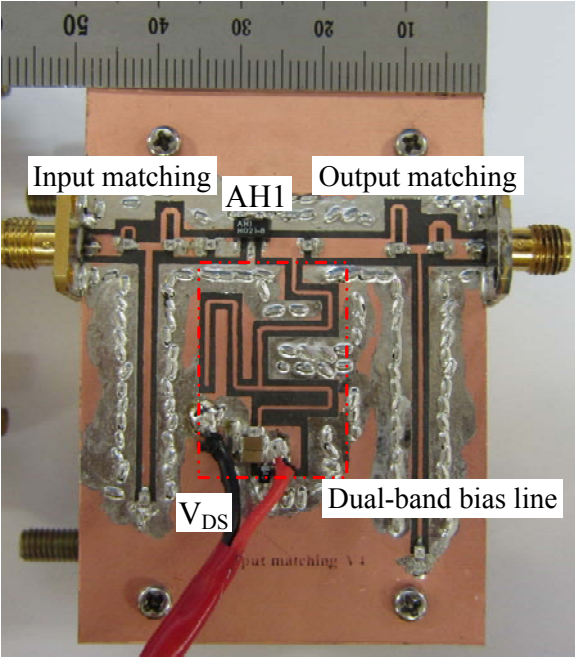


Fig. 4.24. Photograph of the dual-band amplifier with dual-band bias line.

The AH1 is operated with 5 V single supplies. Photograph of the fabricated dual-band amplifier with inductor bias line and dual-band bias line are shown in Fig. 4.23 and Fig. 4.24, respectively. Both are printed on the substrate RT/Duroid-5880 of Rogers. The total size of the fabricated circuits occupies $67 \times 48.6 \text{ mm}^2$ the same. For the proposed dual-band amplifier with dual-band bias line and chip inductor bias get to same results. The saturated output power is 22.33 dBm with gain 12.83 dB and linear gain of 14 dB, as illustrated in Fig. 4.25. The maximum drain efficiency (DE) and PAE are 33.86 % and 32.1%, respectively. The operating frequency is 0.881 GHz.

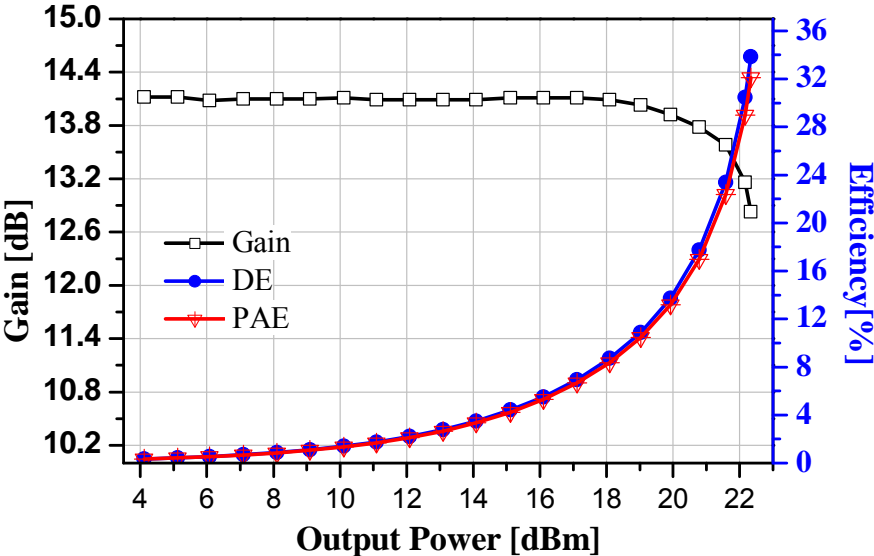


Fig. 4.25. Measured gain and efficiency according to output power with operating frequency 0.881 GHz.

The second band 2.14 GHz, The saturated output power 21.16 dBm with gain 10.66 dB and linear gain of 11.4 dB illustrated in Fig. 4.26. The maximum drain efficiency (DE) and PAE are 23.53 % and 21.51%, respectively.

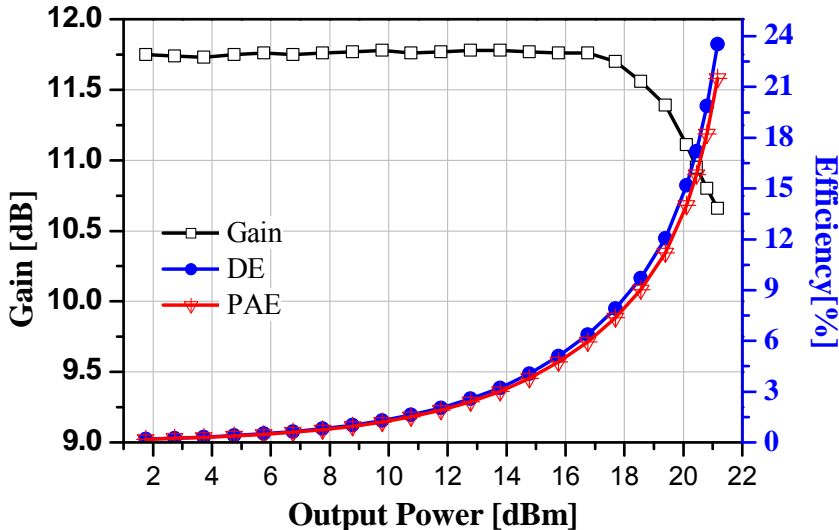


Fig. 4.26. Measured gain and efficiency according to output power with operating frequency 2.14 GHz.

A small signal measurement is done with input power 5 dBm of Network Analyzer *hp* 8720D to validate the out-of-band transmission zeros. Fig. 4.27 shows a measurement result using chip inductor and dual-band bias line.

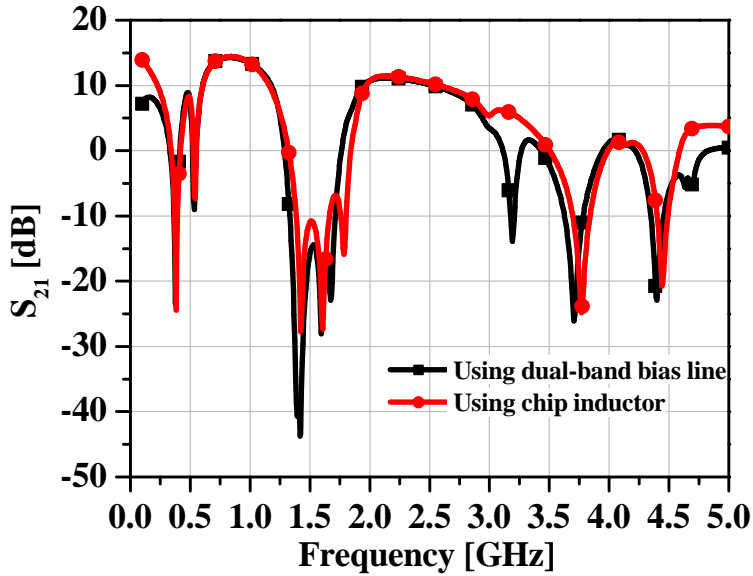
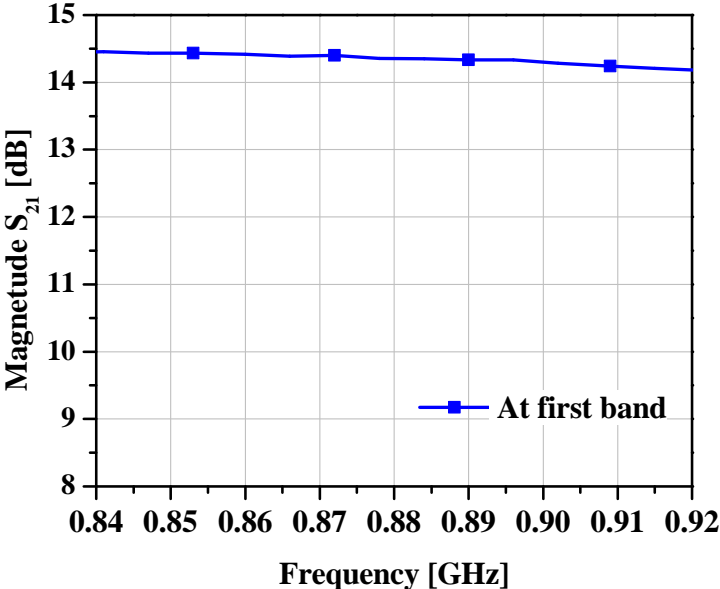


Fig. 4.27. Comparison of the measurement results between using chip inductor and dual-band bias line.

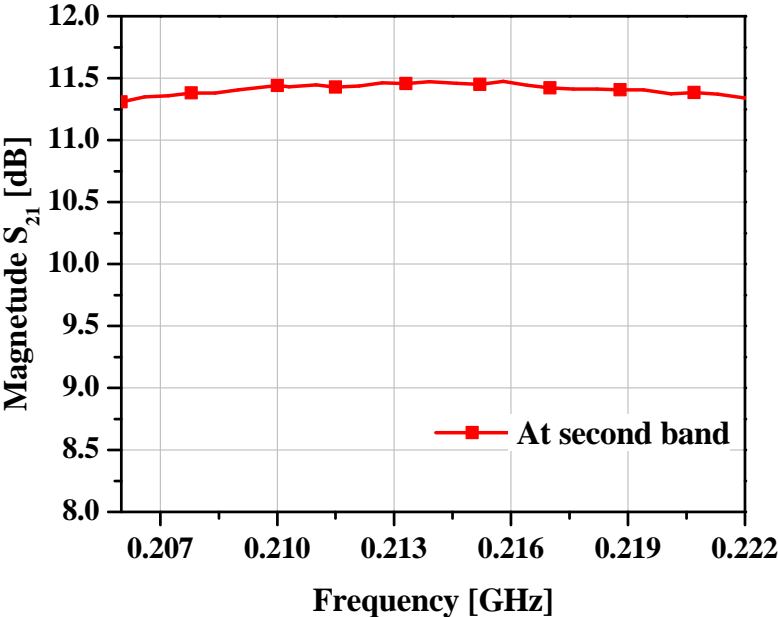
The gain of first band is 14.3 dB with using chip inductor bias and dual-band bias line the same shown in Fig. 4.27. Also, at the second band, we get 11.4 dB. However, dual-band amplifier using dual-band bias line can improve attenuation the out-of-band characteristic. The amplifier using inductor bias line is made seven transmissions zeros out-of-band where the transmission zero at 4.4 GHz is occurred due to the transmission of shunt-series output matching network. However, the amplifier proposed with dual-band bias line is made eight transmission zeros out-of-band. The transmission zero at 3.23 GHz is occurred because of the dual-band bias line. Moreover, the attenuation characteristic is more attenuated the out-of-band excepted two operating frequencies.

Fig. 4.28 shows the flatness characteristic of the operating bands. For the entire bandwidth of GSM (Downlink) (869-894 MHz), the gain is over 14.3 dB shown in

Fig. 4.28(a). At the second band WCDMA base-station (2.11~2.17 GHz), overall gain is over 11.4 dB shown in Fig. 4.28(b).



(a)



(b)

Fig. 4.29. Measurement flatness characteristics: (a) at first band and (b) at the second band.

CHAPTER 5 CONCLUSION

The first key point of this thesis is the understanding of dual-band matching network. Usually, a numbers of matching network are concentrating only impedance matching. However, this dissertation, the dual-band matching network is analyzed with theoretical analysis and can match two impedance of two different frequencies also can make out-of-band transmission zeros. Due to the series-parallel and shunt-series LC, the transmission zeros can be occurred to suppress the unwanted signal. This dual-band amplifier can operate with GSM and WCDMA band of 0.881 GHz and 2.14 GHz frequencies, respectively.

The gain 12.83 dB and 10.66 dB are obtained at 0.881 GHz and 2.14 GHz, respectively. The maximum drain efficiency (DE) at first band and second band are 33.86 % and 23.53%, respectively. Also, the maximum PAE 32.1 % and 21.51 % can be gotten at first band and second band, individually.

Furthermore, dual-band bias line for dual-band amplifier have been derived, simulated, and measured. This dual-band bias line is suitable to use with dual-band active device to feed DC current with noneffective to both fundamental frequencies.

REFERENCES

- [1] L. Wenyuan and W. Hai, "A 0.8-2.1 GHz Broadband Power Amplifier," *International Conference on Communication Technology*, pp. 1050-1053, Sept. 2001.
- [2] H. Sledzik, R. Reber, B. Bunz, P. Schuh, M. Oppermann, M. Muber, M. Seelmann-Eggebert, and R. Quay, "GaN Based Power Amplifier for Broadband Applications from 2 GHz to 6 GHz," *European Microwave Integrated Circuits Conference*, pp. 416-419, Sep. 2010.
- [3] D. Kalin and R. Negra, "Concurrent Planar Multiharmonic Dual-Band Load Coupling Network for Switching-Mode Power Amplifiers," *Microwave Symposium Digest*, pp. 1-4, 2011.
- [4] P. Colantonio, F. Giannini, R. Giofre, and L. Piazzon, "A Design Technique for Concurrent Dual-Band Harmonic Tuned Power Amplifier," *IEEE Trans. Microw. Theory Tech.*, vol. 56, no. 11, pp. 2545-2555, Nov. 2008.
- [5] A. Cidronali, N. Giovannelli, T. Vlasits, R. Hernaman, and G. Manes, "A 240W Dual-Band 870 and 2140 MHz Envelope Tracking GaN PA Designed by a Probability Distribution Conscious Approach," *Microwave Symposium Digest (MTT)*, pp. 1- 4, 2011.
- [6] K. Rawat and F. M. Ghannouchi, "Dual-Band Matching Technique Based on Dual-Characteristic Impedance Transformers for Dual-Band Power Amplifier

- Design,” *IET Microw. Antennas Propag.*, vol. 5, iss. 14, pp. 1720-1729, May. 2011.
- [7] P. Wright, J. Lees, J. Benedikt, P. J. Tasker, and S. C. Cripps, “A Methodology for Realizing High Efficiency Class-J in a Linear and Broadband PA,” *IEEE Trans. Microw. Theory Tech.*, vol. 57, no. 12, pp. 3196-3204, Dec. 2009.
- [8] J. Lim, Y. Jeon, S. M. Han, Y. Jeong, and D. Ahn, “A Design of Dual Band Amplifiers Using CRLH Transmission Line Structure,” *IEICE Trans. Electron.*, vol. E95-C, no. 5, pp. 964-967, May. 2012.
- [9] S. H. Ji, C. S. Cho, J. W. Lee, and J. Kim, “Concurrent Dual-Band Class-E Power Amplifier Using Composite Right/Left-Handed Transmission Lines,” *IEEE Trans. Microw. Theory Tech.*, vol. 55, no. 6, pp. 1341-1347, Jun. 2007.
- [10] S. H. Ji, G. S. Hwang, C. S. Cho, J. W. Lee, and J. Kim, “836 MHz/1.95GHz Dual-Band Class-E Power Amplifier Using Composite Right/Left-Handed Transmission Lines,” 36th European Microwave Conference., pp. 356-359, Sep. 2006.
- [11] S. C. Cripps, *RF Power Amplifier for Wireless Communications*. Boston, MA: Artech House, pp. 41-43, 2006,
- [12] D. M. Pozar, *Microwave Engineering* 4th ed. New York: Wiley, pp. 415-416, 2012.

- [13] S. Park, H. Choi, and Y. Jeong, "Microwave Group Delay Time Adjuster Using Parallel Resonator," *IEEE Microw. And Wireless components Letters.*, vol. 17, no. 2, pp. 109- 111, Feb. 2007.